ELECTRON BEAM MOLECULAR LASERS

S. R. Byron

Mathematical Sciences Northwest, Incorporated

Prepared for:

Advanced Research Projects Agency

November 1972

MATHEMATICAL SCIENCES NORTHWEST, INC.
4545 15th AVENUE N.E. SEATTLE, WASHINGTON 98105

MSNW Report No. 72-105-1

SEMI ANNUAL TECHNICAL REPORT

ELECTRON BEAM MOLECULAR LASERS

Prepared by

Mathematical Sciences Northwest, Inc.
4545 Fifteenth Avenue N.E.
Seattle, Washington 98105

November 1972

Contract N00014-72-C-0430

Sponsored by

Advanced Research Projects Agency
ARPA Order No. 1807

Monitored by

Office of Naval Research
Code 421

ARPA ORDER NO.: 1807 Amend.1

PROGRAM CODE: 2E90

NAME OF CONTRACTOR: Mathematical Sciences Northwest, Inc.

EFFECTIVE DATE OF CONTRACT: 15 March 1972 - 15 November 1972

CONTRACT AMOUNT: $270,109.00

CONTRACT NUMBER: N00014-72-C-0430

PRINCIPAL INVESTIGATOR: Dr. S. R. Byron
206-524-9300

SCIENTIFIC OFFICER: Director, Physics Programs
Physical Sciences Division
Office of Naval Research
Department of the Navy
800 North Quincy Street
Arlington, Virginia 22217

ACKNOWLEDGMENT

In addition to the principal investigator, contributions were made by Dr. Walter Christiansen, Mr. George Mullaney, Dr. Leonard Nelson, and Mr. Albert Pindroh, as well as Mr. Gary Loda, then of Physics International.

This research was supported by the Advanced Research Projects Agency of the Department of Defense, and was monitored by ONR under contract number N00014-72-C-0430.

ABSTRACT

An experimental and theoretical study has been initiated on the application of electron-beam-stabilized electrical discharges to the excitation of infrared laser emission from HF and DF molecules. Electric discharge pumping of H_2 or D_2 vibration is utilized, together with near-resonant V-V transfer to HF or DF. The large anharmonicity of these molecules leads to a non-Boltzmann vibrational population distribution which can provide a partial inversion in the upper vibrational levels as is found in CO electric discharges. Initial experimental observations of HF fluorescence and absorption in argon, hydrogen, hydrogen fluoride mixtures at 0.25 atm and room temperature confirm the basic principles involved. A detailed analytical model indicates that H_2 rotational excitation and H_2 electronic excitation leading to dissociation are significant problems and must be overcome by using high electrical discharge current and low electric field strength. This requires a high current electron beam ($\sim$ 100 to 200 ma/cm^2) for a pulse duration of 10 to 20 μsec. A 5 cm by 50 cm electron gun having this capability is currently being constructed.

During the initial experimental studies of HF fluorescence it was found that repetitive pulses were emitted from H_2 and N_2 in the 1 to 2 micron wavelength region and from N_2 in the 3000 to 4000 Å region. The emission characteristics depend critically on the concentration of HF present and also require a high value of applied electric field strength. The emission has been identified as the first and second positive bands

of N_2 and a similar electronic band of H_2. The use of gold coated mirrors indicated weak laser action on the first positive band of N_2 and on the infrared emission of H_2; the emission pulse duration was about 10 μsec.

An additional task was carried out under this contract to evaluate the possibility of generating long duration, high energy density laser pulses on various molecules, particularly CO_2. Measurements were made of optical disturbances induced by the electrical discharge, electron beam requirements and arc formation at high pressure, and optical gain at high pressure. It was concluded that long pulse duration, high pressure operation appears to be feasible, but will require further research on several problem areas.

TABLE OF CONTENTS

LIST OF TABLES

LIST OF FIGURES

SECTION I

INTRODUCTION

A major advance in high energy density pulsed gas lasers resulted from the development of large area, high voltage electron beams to stabilize high pressure, large volume electrical discharges (Refs. 1 and 2). This approach was first applied to CO_2 lasers and has recently been extended to cryogenic CO lasers. At the same time considerable attention was directed toward the development of high power chemical lasers which have been based primarily on reactions that produce HF or DF (Refs. 3 and 4). It was recognized at Mathematical Sciences Northwest, Inc. that HF and DF molecules could be pumped in an electron-beam-stabilized electrical discharge in much the same way that CO_2 and CO have been and could yield high energy density laser pulses at 2.8 to 3.0 microns and at 3.8 to 4.1 microns. This program was then initiated to explore this possibility.

There are several advantages of utilizing DF rather than CO_2 or CO as the laser molecule in an electrical discharge laser; there are also several disadvantages. The principal advantage of DF is the high transmission characteristics of the atmosphere at 3.7 to 4.0 microns. In addition, the DF laser (like the CO laser) is based on a partial inversion and thus has a much higher quantum efficiency limit than CO_2. Furthermore, it should be possible to achieve good laser performance with DF initially at room temperature because of its large anharmonicity and large rotational spacing; CO on the other hand must be operated at cryogenic temperatures ($\sim$ 100° K). The principal disadvantage of DF is the high VT

collisional decay rate of vibrational energy. In our approach this is overcome by utilizing gas mixtures that contain only a few percent DF. Efficient transfer of electrical discharge energy to vibrational energy is achieved by including in the gas mixture 10 to 20 percent D_2 which has a close vibrational level coincidence with DF.

The investigation of HF and DF in this program has centered heavily on the HF molecule for two reasons. First, there are very few suppliers of DF and the purity of the product is inferior to that achieved for HF. Second, the vibrational relaxation processes of HF and H_2 have been investigated much more thoroughly in recent years than have those of DF and D_2. Thus a good correlation between theory and experiment will be achieved earlier with HF and will lead most rapidly to a thorough understanding of the principles involved. However, a few exploratory experiments were conducted with DF and are reported here. The results of the analytical and experimental studies of HF and DF electrical discharge laser technology are described in Section II.

To carry out this program a cooperative effort was established between Mathematical Sciences Northwest, Inc. (MSNW) and Physics International (PI). The laser technology was provided by MSNW, while PI supplied the thermionic electron beam and power supply, and the electrical discharge power supply and timing circuitry. The program included a joint effort between MSNW and PI to study the characteristics of electron-beam-stabilized electric discharges, with particular emphasis on high pressure, long pulse duration operation. Recently this joint effort has been terminated, and the equipment has been purchased by MSNW from PI. The results of the small scale experimental study of high pressure, long duration e-beam stabilized discharges are described in Section III.

Unexpectedly, during the initial experimental studies of HF fluorescence, a series of repetitive pulses was observed in the near infrared region of the spectrum. These appeared near the first vibrational overtone of HF and were initially misinterpreted as being due to such radiation in HF. Through subsequent spectral analysis and additional exploratory experiments, it was found that these emission pulses originate from excited electronic states of H_2. It was also discovered that similar pulses occur when 10 to 20 percent N_2 rather than H_2 is used in the gas mixture. These pulses were seen at 1 to 1.5 microns (N_2 first positive band) and also at 3371 to 4058 Å (N_2 second positive band). The appearance, magnitude, duration, and repetition rate of these pulses were found to depend critically on the amount of HF in the gas mixture, although only 0.5 to 3 percent HF was used. These results have been summarized in a manuscript submitted for publication in Applied Physics Letters (to appear 15 January 1973). As yet there is no detailed explanation of the effects although it is thought that electronic energy transfer plays a significant role. The observations and possible interpretations are described in detail in Section IV.

The study of HF and DF electric discharge laser possibilities and further investigation of the N_2 electronic transfer laser possibilities are being continued on the current program.

SECTION II

HF AND DF ELECTRIC DISCHARGE LASER TECHNOLOGY

2.1. General Description

This program is directed toward an investigation of the properties of V-V pumped, infrared active diatomic molecules for use in electric discharge lasers. Previous work (Ref. 5) has shown that V-V pumping is effective in producing a partial inversion of CO and leads to high efficiency conversion of electrical energy to laser energy. In some cases the CO vibrational temperature is increased and laser efficiency is improved by including a significant fraction of N_2 in the gas mixture.

In the investigation described here this laser principle is extended to other diatomic molecule pairs such as HF and H_2, DF and D_2, HCl with D_2, and DCl with N_2 or CO. In each case the pair of diatomic molecules is composed of an infrared inactive molecule and an infrared active molecule which have reasonably close coincidence of vibrational energies. The vibrational mode of the infrared inactive molecule is excited by electron impact in an electrical discharge that is controlled and stabilized by an external ionization source. The vibrational energy of the inactive molecule is transferred by V-V collisions to the infrared active molecule and a partial inversion may be produced in the upper vibrational levels of the infrared active molecule.

The spectroscopic constants of a number of candidate molecule pairs are given in Table II-1. Table II-2 contains current information on VV and VT rates of the lowest vibrational level of the laser molecule. The

Table II-1

Spectroscopic Constants for Several Candidate Partial Inversion Infrared Laser Molecules

Pump Molecule	θ_v, °K	$\Delta\theta_v$, °K	Laser Molecule	θ_v, °K	$\Delta\theta_v$, °K	θ_r, °K	Emission Region, μ	VT Decay(300° K) μsec-atm
N_2	3353	41.5	CO	3076	38.6	2.76	4.8 - 6	$> 10^6$ (Ref. 6)
H_2	5985	342	HF	5697	256	30	2.7 - 3	.024 (Ref. 7)
D_2	4300	184	DF	4180	131	15.8	3.7 - 4	.055 (Ref. 8)
D_2	4300	184	HCl	4150	117	15	3.7 - 4	1.6 (Ref. 9)
N_2	3353	41.5	DCl	3010	78	7.8	5 - 6	6.0 (Ref.10)

Table II-2

Vibrational and Rotational Relaxation Times in $HF/H_2/A$ Mixtures at 300° K

	p τ, μsec-atm
VT DECAY	
$HF + HF(v) \rightarrow HF + HF(v-1)$	$0.024/v$
$H_2 + HF(v) \rightarrow H_2 + HF(v-1)$	$0.8/v$
$H_2(v) + HF \rightarrow H_2(v-1) + HF$	-
$H_2(v) + H_2 \rightarrow H_2(v-1) + H_2$	$10^3/v$
VV TRANSFER	
$HF(1) + HF(1) \rightarrow HF(2) + HF(0)$	0.001
$H_2(1) + HF(0) \rightarrow H_2(0) + HF(1)$	0.021
$H_2(1) + H_2(1) \rightarrow H_2(2) + H_2(0)$	not known
ROTATIONAL RELAXATION	
$H_2(Rot) + H_2$	0.0175 μsec atm
$HF(Rot) + H_2$	"

H_2-HF system has the favorable characteristics of large anharmonicity, $\Delta\theta_v$, and large rotational energy level spacing, θ_R, but HF has the unfavorable characteristic of short VT decay time, τ_{VT}. The D_2-DF and D_2-HCl systems have smaller values of θ_V and θ_R, but larger values of τ_{VT}. By comparison the N_2-CO system has very small values of θ_V and θ_R, but very large values of τ_{VT}.

The effect of these parameters is illustrated by an approximate criterion for a partial inversion in the laser molecule, given by

$$T_{V'} > \theta_{V'}(T_R/4\theta_R)^{\frac{1}{2}} \qquad (1)$$

where $T_{V'}$ represents the effective vibrational temperature based on the population of the lasing level, V', relative to the next lower vibrational level, $V'-1$. The value of $T_{V'}$ required by Equation (1) for CO at 100° K is about the same as that required for HF, DF, HCl, or DCl at 300° K. Thus the spectroscopic constants indicate that electric discharge lasers may be achieved at room temperature in the hydrogen and deuterium halides.

In order to reach the required value of $T_{V'}$ in these gases, it is necessary that the V-V collisional transfer rates must exceed the VT decay rates by a large margin. It is seen in Table II-2 that the ratio for HF of about 25 is much larger than 1, although it is considerably smaller than the value of about 10^5 for CO at room temperature. The effect of the ratio of the VV rate to that of the VT rate in the hydrogen and deuterium halides is one of the key questions being addressed in this program and is discussed in more detail in Section 2.2.

A second requirement in achieving a high vibrational temperature, T_V, in the gas mixture is efficient transfer of the electric discharge energy to molecular vibration. The cross section for electron impact excitation of the V=1 level of H_2 (Ref. 11) is compared in Figure 1 with the integrated cross section for the first 8 levels of N_2 (Ref. 12). Excitation of the V=2 level of H_2 is an order of magnitude smaller than that for V=1. It is seen that the peak cross section for H_2 vibration is about one-seventh that for N_2 vibration, although the H_2 cross section covers a wider range of electron energy. The efficiency of vibrational pumping of H_2 in an electric discharge is then dependent on the relative magnitude of the competing energy loss processes. These include elastic collisions, rotational excitation, and electronic excitation. The inelastic cross sections for rotational excitation (Ref. 11) and for excitation of the lowest electronic state, the repulsive $b^3\Sigma_u^+$ state of H_2 (Ref. 13) are also shown in Figure 1. It is apparent that very low electron energies or very high electron energies would be inefficient in exciting H_2 vibration. In Section 2.2 a detailed analysis of this problem is described, and it is shown that satisfactory vibrational excitation can be achieved over a range of intermediate electron energies; the maximum vibrational pumping efficiency of H_2 is about 70 percent.

Since the preceding discussion indicates that the basic requirements for producing a partial inversion laser on HF, DF, HCl, or DCl appear (qualitatively) to be met, it is natural to ask why this has not been accomplished previously in the laboratory. There are two principal reasons.

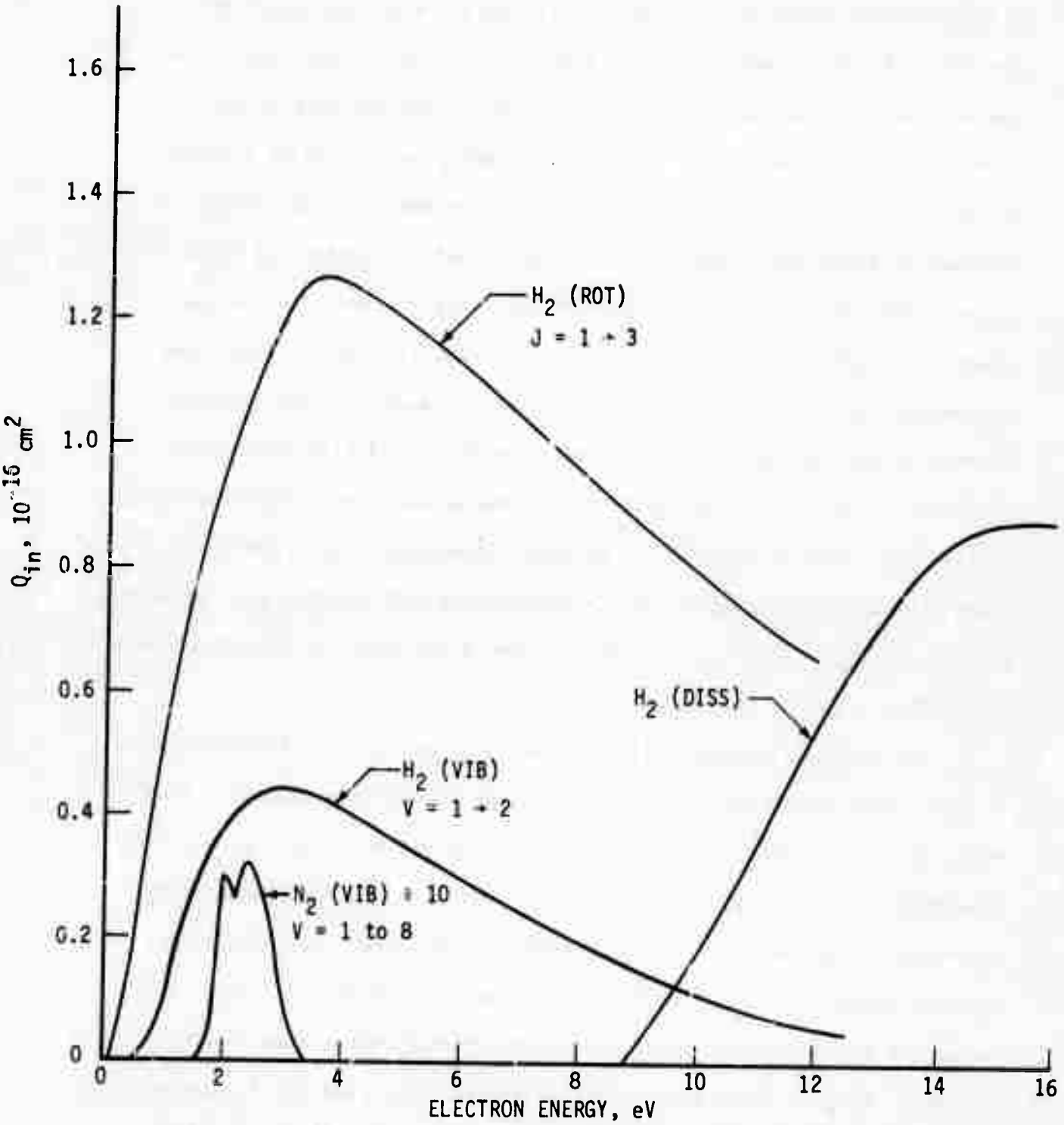

FIGURE 1. Inelastic Cross-sections for Electron Impact with Hydrogen

The first reason is associated with the low lying, repulsive excited electronic states of these molecules. In self-sustained electric discharges, the electron energy must be sufficiently high to produce the required rate of ionization. Under these conditions a large fraction of the discharge energy produces molecular dissociation and only a small fraction goes into molecular vibration. In addition, the atoms then add to the already rapid VT decay rate. It is therefore essential to use an external ionizing source and a low electric discharge voltage in order to achieve high vibrational excitation and low dissociation. The second reason is associated with the relatively low electron impact vibrational excitation cross section and the large VT decay rates of these molecules. In order to achieve a vibrational pumping rate that sufficiently exceeds the VT decay rate, it is necessary to provide an electron density of the order of 10^{13} cm^{-3} or more in the electric discharge. Only recently have external ionizing techniques been developed that will provide the required electron density. With this new technology, a new class of molecular laser possibilities may be realized.

One additional physical process plays a key role in the development of these laser possibilities. Since an external ionizing source is necessary, the requirements on this source may be affected strongly by electron attachment losses to HF, DF, HCl, or DCl. For example, the dissociative attachment cross section for HCl is about 2×10^{-18} cm^2 (Ref. 14) at an electron energy of 0.5 to 1 e.v. Thus a partial pressure of 2 Torr of HCl in the gas mixture will lead to an electron density decay time of about 10^{-7} sec. This is about a factor of 10 shorter than that due to dissociative

recombination (for an electron density of 10^{13} cm^{-3}) and will require a corresponding factor of 10 increase in the strength of the source of external ionization. Due to the greater bond strength of HF and DF, this effect is much smaller and has very little impact on the requirements of the external ionization source. This has been verified experimentally as discussed in Section 2.3.2.

A more detailed analysis of this concept as it applies to H_2-HF mixtures is given in Section 2.2. A series of initial exploratory experiments is described in Section 2.3 which serves to confirm the basic principles involved. However, the electron beam current density was not sufficient in these experiments to provide the necessary electron density and electric discharge power input rate to achieve laser emission. A higher current electron beam is presently under construction.

2.2. Analytical Model for $HF/H_2/Ar$ Gas Mixtures

A detailed analytical model is being developed for the electric discharge excitation of HF and DF laser molecules. The model contains 3 major components:

1. Determination of the electron distribution function and the resulting electrical discharge excitation rates of rotation, vibration, electronic excitation, ionization, and elastic transfer.
2. Determination of the population of vibrational and rotational levels throughout the excitation pulse.
3. Determination of optical gain and saturated power extraction.

These components are being developed first for $HF/H_2/Ar$ gas mixtures for use in comparing with experimental observations. The progress achieved on modeling of $HF/H_2/Ar$ gas mixtures is described in Section 2.2.1 and plans for more detailed modeling are outlined in Section 2.2.2.

2.2.1. Initial Kinetic Model of $HF/H_2/Ar$ Electric Discharge Laser

a. Time dependent solution (simplified model)

A simplified kinetics model has been developed to study the vibrational relaxation of H_2 and HF in the presence of Ar. The anharmonic oscillator model was used to describe the vibrational levels of H_2 and HF. The number of vibrational levels considered for both gases was six (ground level plus first five excited states).

Relaxation mechanisms considered were intra- and inter-molecular V-V transfer and V-T decay. In addition the rotational relaxation of H_2 and HF was considered since the rotational relaxation times are comparable to the time scale of vibrational relaxation, and are important for determining the gain coefficients which are a function of the rotational distribution.

In the simplified model both HF and H_2 intra-molecular V-V transfer, only the first excited level was allowed to pump the higher levels, e.g.

$$M(v=1) + M(v=n) \rightleftarrows M(v=0) + M(v=n+1) \qquad (2)$$

$$n = 1 \text{ to } 4$$

The inter-molecular V-V transfer mechanism was limited to the exchange of one quantum from the first excited level of H_2 with HF, e.g.

$$H_2(v=1) + HF(v=n) \rightleftarrows H_2(v=0) + HF(V=n+1) \qquad (3)$$

$$n = 0 \text{ to } 4$$

In the case of V-T relaxation, the following mechanisms were included:

$$HF(v) + HF \rightleftarrows HF(v-1) + HF \qquad (4)$$

$$HF(v) + H_2 \rightleftarrows HF(v-1) + H_2 \qquad (5)$$

$$H_2(v) + H_2 \rightleftarrows H_2(v-1) + H_2 \qquad (6)$$

The kinetics of the rotational energy were treated by assuming a Boltzmann distribution of the rotational energy at one rotational temperature for both H_2 and HF. For simplification only H_2 was considered as a catalyst in the rotational relaxation of H_2 and HF, and it was assumed their relaxation times were equivalent.

The system of equations to be solved for constant density cases are:

$$\frac{dN_i(v)}{dt} = \left(\frac{dN_i(v)}{dt}\right)_{V-V} + \left(\frac{dN_i(v)}{dt}\right)_{V-T} + \left(\frac{dN_i(v)}{dt}\right)_{\substack{\text{electronic} \\ \text{pumping}}} \tag{7}$$

$$\frac{dE_{Rot}}{dt} = \frac{1}{\tau_{Rot}}\left[E(t) - E(T_R)\right] + \left(\frac{dE_{Rot}}{dt}\right)_{\substack{\text{electronic} \\ \text{pumping}}} \tag{8}$$

$$\frac{dT}{dt} = -\frac{1}{C_v}\left[\sum_{i,v} E_i(v)\,\frac{dN_i(v)}{dr} + \left(\frac{dE_{Rot}}{dt}\right) - \frac{dE_{pump}}{dt}\right] \tag{9}$$

where: $E_i(v)$ = energy of level v for species i

$\frac{dE_{pump}}{dt}$ = energy input by electronic pumping

C_v = translational heat capacity at constant volume

$N_i(v)$ = density of vibrational level v of species i

T_R = rotational temperature

Note: Vibrational pumping mechanism limited to excitation of ground state H_2 to the first excited level of H_2.

The relaxation times used in the above system of equations are given in Table II-2.

b. Steady state solution

A steady state solution for conditions of vibrational nonequilibrium in gas mixtures of H_2, HF, and Ar was obtained from the master vibrational equations at a constant translational and rotational temperature for a specified vibration excitation rate of H_2 from the ground to the first vibrational level. The master equations used are similar in form to those developed for CO by Caledonia and Center (Ref. 15).

The master vibrational rate equation for the concentration of species N in the i^{th} vibrational level, in the presence of species M with which it can exchange vibrational energy and species K which contribute to VT decay only, is

$$\frac{dN_i}{dt} = Z_{NN} \sum_j \left[P^{i-1,i}_{j,j-1} N_{i-1} + P^{i+1,i}_{j,j+1} N_{j+1} - \left(P^{i,i-1}_{j,j+1} + P^{i,i+1}_{j,j-1} \right) N_i \right] N_j$$

$$+ Z_{NM} \sum_m \left[P^{i-1,i}_{m,m-1} N_{m-1} + P^{i+1,i}_{m,m+1} N_{m+1} - \left(P^{i,i-1}_{m,m+1} + P^{i,i+1}_{m,m-1} \right) N_i \right] N_m$$

$$+ \sum_K^{\text{all species}} Z_{NK} N_K \left[P^{i-1,i}_{VT,K} N_{i-1} + P^{i+1,i}_{VT,K} N_{i+1} - \left(P^{i,i-1}_{VT,K} + P^{i,i+1}_{VT,K} \right) N_i \right]$$

$$+ \left(\frac{dN_i}{dt} \right)_{\text{electronic}} \qquad (10)$$

where Z_{NN}, Z_{NM}, and Z_{NK} are the collision frequencies of species N colliding with N, M, and K, respectively, at unit concentrations. The probabilities of reaction, $P^{i,i\pm1}_{j,j\pm1}$ and $P^{i,i\pm1}_{VT,K}$ refer to the V-V and V-T

exchange, respectively. The vibrational excitation rate due to collision with electrons is given by a fixed source term, $\left(\frac{dN_i}{dt}\right)_{electronic}$. Forward and reverse rates were related through the principle of detailed balancing.

This system of equations was solved for the steady state by the Newton-Raphson iterative method for a fixed translational temperature of 300° K, and an electronic pumping rate for the vibrational excitation of the ground level to the first vibrational level of H_2 which specified a fixed temperature of 2700° K between these two levels. The 2700° K temperature was chosen since the unsteady state solution led to this level of temperature for a 20 μsec pulse at a pumping rate of 1500 watts/cm^3. The gas concentrations were 1% HF, 10% H_2, 89% Ar. Twelve vibrational levels were used for both the HF and H_2, with the twelfth level being a reflecting boundary in each case.

A comparison of the HF vibrational population distribution obtained from the two methods of solution, using the same vibrational rates in both solutions, is shown in Figure 2. It is seen that the unsteady terms are significant throughout the pulse duration; a pumping time of 10 to 15 μsec is needed to approach the steady state population distribution. It is also seen that a total inversion cannot be achieved under these conditions; this is because the VT rates of the upper vibrational levels represent a significant loss with respect to the VV pumping rates. A partial inversion can be achieved, however, and is discussed further in Section 2.2.1e.

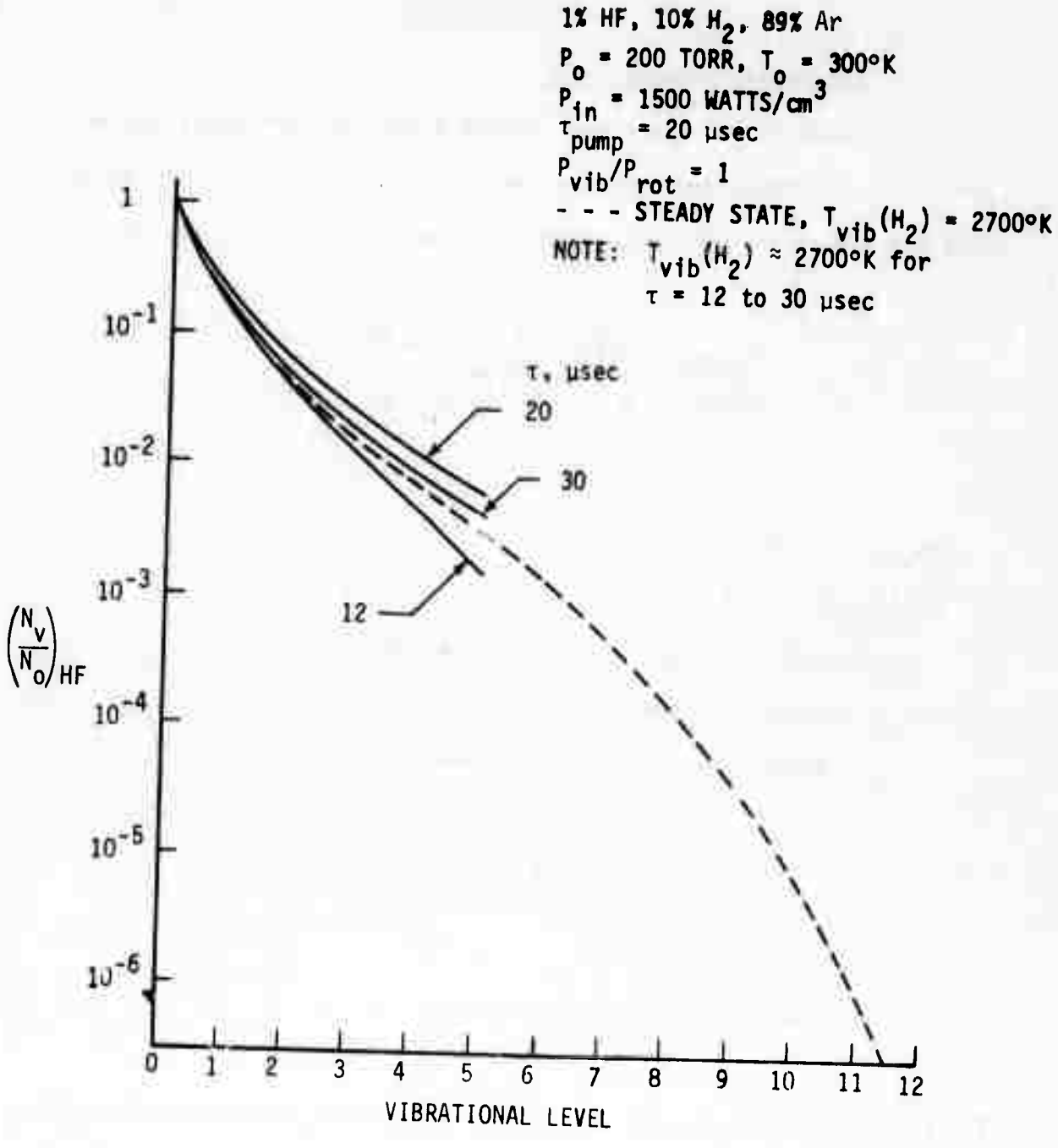

FIGURE 2. Computed HF Vibrational Level Populations in an Electric Discharge

c. Electronic pumping rates

The ratio of the electrical energy going into the first vibrational level of H_2 to that going into the rotational level ($J = 1 \rightarrow 3$) was computed for a Maxwell distribution for the electrons. This ratio is given by

$$\frac{E_{(vib)}}{E_{Rot}} = \frac{\varepsilon_{vib} \int_0^\infty u\, f_m\, Q_{vib}\, du}{\varepsilon_{rot} \int_0^\infty u\, f_m\, Q_{rot}\, du} \qquad (11)$$

where:

ε_{vib} = 0.515 ev

ε_{rot} = 0.069 ev

Q_{vib} = inelastic cross section for $v = 0 \rightarrow 1$

Q_{rot} = inelastic cross section for $J = 1 \rightarrow 3$

f_m = Maxwell distribution function

$$f_m = \frac{2}{\sqrt{\pi}} (T_e)^{-3/2} \exp(-\frac{u}{T_e})$$

for u in ev

and T_e = electron temp in ev

The inelastic cross sections are given in Figure 1, and the energy ratios are given in Figure 3.

The results of Figure 3 have not been carried beyond an average electron temperature of 1 ev because of the increasing contribution of dissociation and electronic excitation beyond this point. These effects

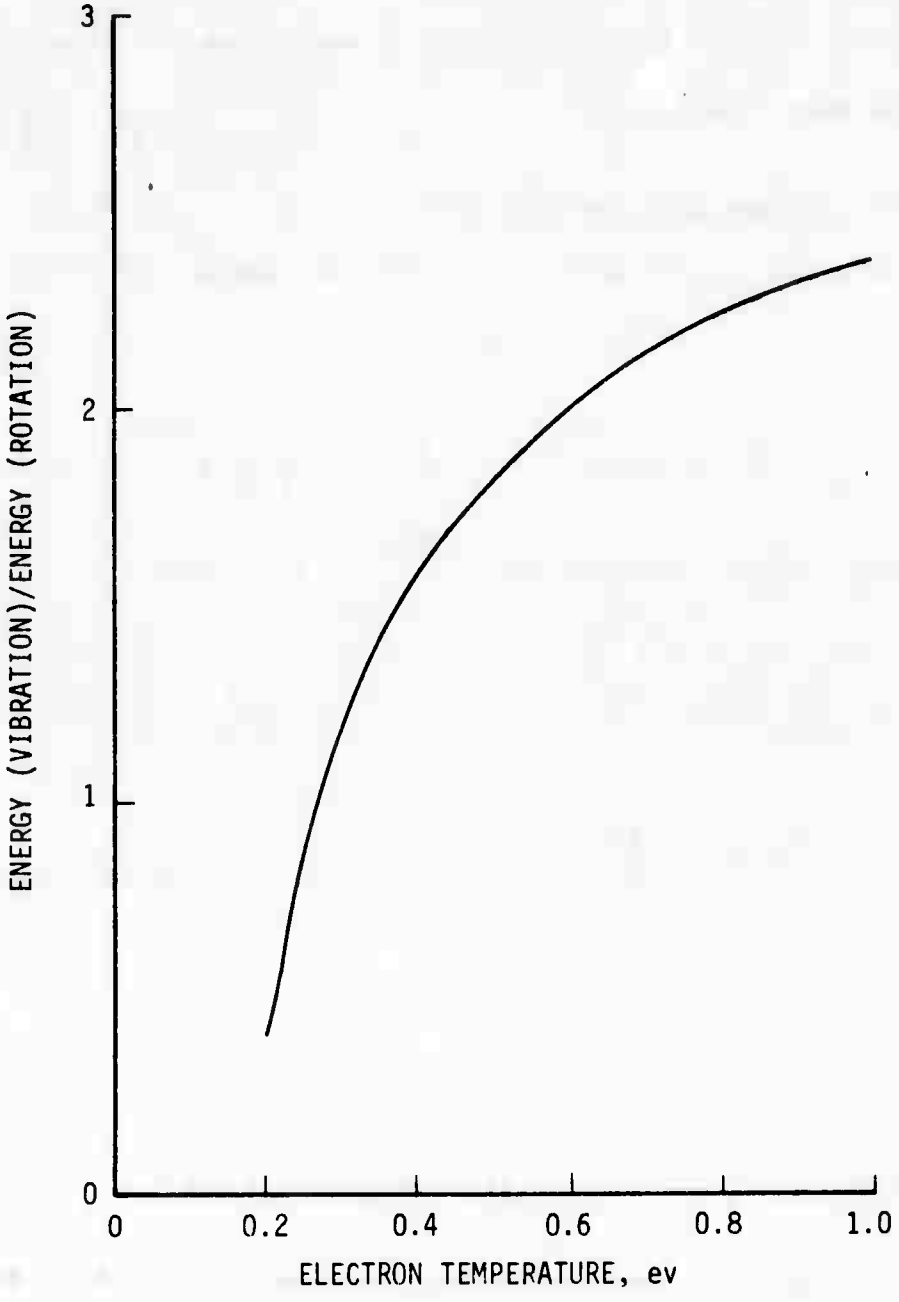

FIGURE 3. H_2 Pumping Ratio for Maxwell Distribution

are currently being incorporated in a computerized solution to the Boltzmann equation describing the electron energy distribution function. For purposes of the gain calculations described in Section 2.2.1e, it is assumed that half the electrical discharge power goes into vibration and half goes into rotation.

d. Optical gain and line shift

The small signal gain, g_o, at the line center for a P(J) transition $(v + 1 \rightarrow V;\ J - 1 \rightarrow J)$ is given by

$$g_o = \frac{\lambda^2_o}{8\pi} A \frac{\theta r}{T} (2J-1) e^{\frac{-J(J-1)\theta r}{T}} \left[1 - \frac{n(v)}{n(v+1)} e^{\frac{-2J\theta r}{T}}\right] n(v+1) G(\nu_o) \quad (12)$$

where $G(\nu_o)$ = line shape function = $\frac{2\sqrt{\ell n\ 2}}{\sqrt{\pi}\ \Delta\nu_D} e^a \operatorname{erfc}(a)$

$$a = \frac{\Delta V_c}{\Delta V_D} \sqrt{\ell n\ 2}$$

$$\Delta\nu_D = \left[\frac{8\ kT\ \ell n\ 2}{M}\right]^{\frac{1}{2}} \frac{1}{\lambda_o}, \text{ Doppler full width at half maximum}$$

$$\Delta\nu_c = \frac{\nu_c}{\pi}, \text{ Lorentz full width at half maximum in } sec^{-1}$$

A = transition probability (inverse lifetime)

n(v) = molecular density for vibrational level v

The Lorentz broadening is due to the collisions of the HF with itself and with other species present in the mixture (H_2 and Ar), and is given by

$$\nu_c = \sum_i x_i \sqrt{\frac{8kT}{\pi\mu_{HF-i}}}\, Q_{(HF-i)}$$

where μ_{HF-i} = reduced mass

and $Q_{(HF-i)}$ = optical broadening cross section

For a mixture $\Delta\nu_c = \Sigma x_i \, \Delta\nu_{c(HF-i)}$

In Figure 4 the half-widths (1/2 of the full width at half maximum) for HF self broadening, H_2 broadening, and Ar broadening are plotted versus $|m|$, where $|m| = J$ for P-branch transitions, and $|m| = J + 1$ for R-branch transitions.

It is seen that the HF self-broadening has the character of the resonant dipole interaction model, although the theory over-estimates the broadening for low $|m|$ values.

The room temperature data of Levell and Herget (Ref. 16) were used for the self-broadening of HF, with the temperature dependence determined by the theoretical resonant dipole-billiard ball model (Ref. 17) fitted to their data. Collision broadening by H_2 and argon was based on the data of D. F. Smith (Ref. 17) at 100° C, with the temperature dependence scaled by $T^{-\frac{1}{2}}$, which assumes constant broadening cross sections (Ref. 18).

In the measurement of the gain (absorption) of HF mixtures containing argon, the effect of the line shift due to argon must be considered since the line center of the mixture may not coincide with the probe line center. This line shift is comparable to the Lorentz half-width, which would result

in the probe laser measuring about 1/2 of the line gain (absorption) at the line center. The line shifts due to the presence of Ar and HF are given in Table II-3. These line shifts were scaled with a $T^{-\frac{1}{2}}$ dependence based on the data of Ref. 18.

Table II-3

Frequence Shift of HF Lines by HF and Ar Collisions

Line	Line Shift (cm^{-1}/atm)	
	(a) HF-Ar (Ref 4)	(b) HF-HF (Ref 3)
R(0)	+ 0.0128	+ 0.036
R(1)	- 0.0198	not measured
R(2)	- 0.0222	- 0.012
R(3)	- 0.0259	not measured
R(4)	- 0.0280	- 0.018
R(5)	- 0.0289	- 0.014

(a) T = 20° C

(b) T = 100°C

e. Gain calculation

The gain for a 1% HF, 10% H_2, 89% Ar mixture was obtained from the time dependent solution for various energy input rates from 900 to 3000 watts/cm^3 and for 20 μsec duration. This energy was divided equally

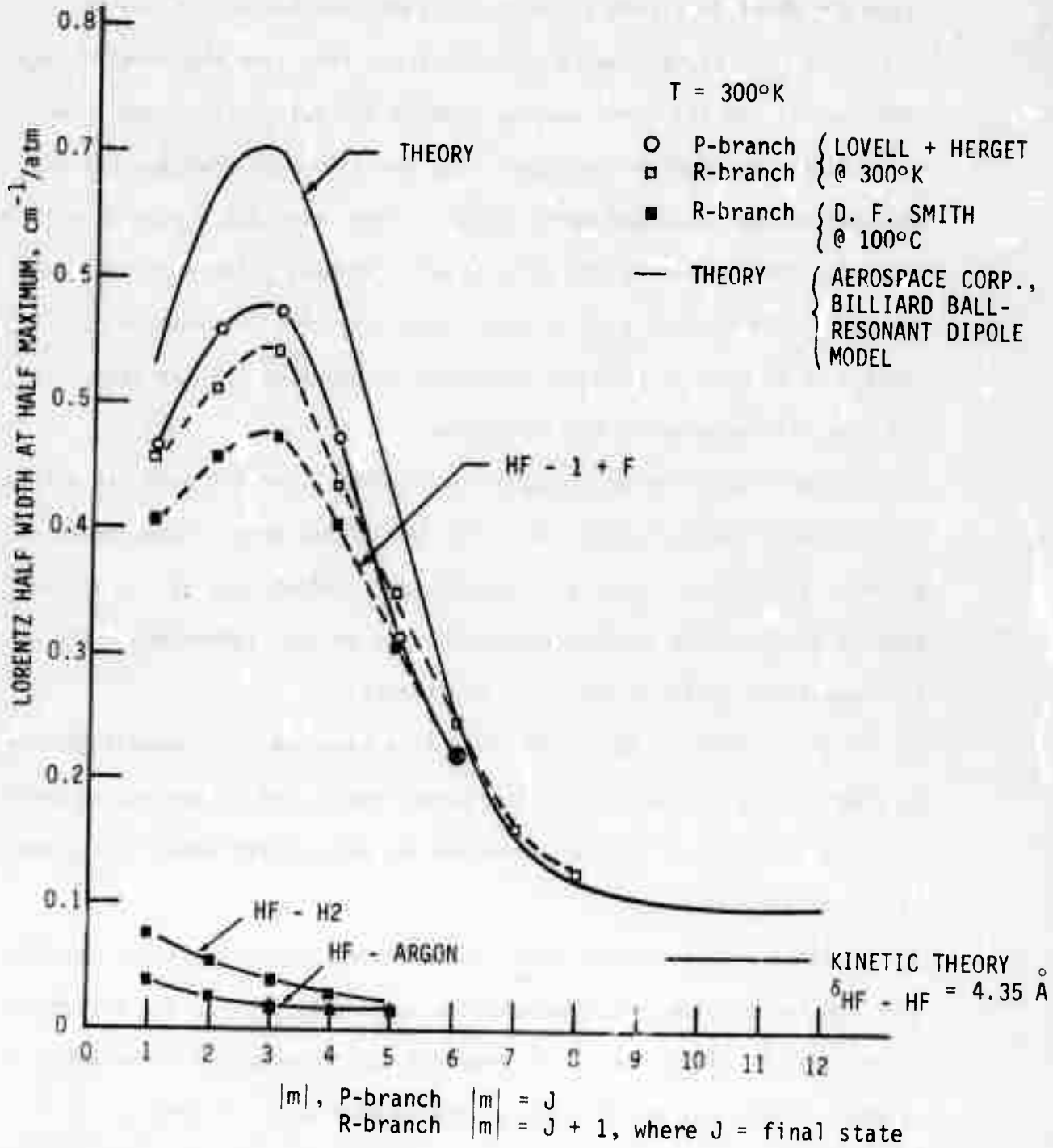

FIGURE 4. HF Lorentz Broadening

between the H_2 vibration and rotation. Results for these energy input rates are shown in Figure 5, where the gain coefficient for the HF ($v = 3 \rightarrow v = 2$) transition is plotted versus time from the onset of the input pulse. At the lower pumping rate of 900 watts/cm^3 there is no significant gain during the pulse. For the 1500 watts/cm^3 pumping rate the gain becomes positive after 14 to 17 μsec, reaching a peak of ≈ 1%/cm following termination of the input power. Highest gains were obtained for the 3000 watts/cm^3 pumping rate, which switched to positive gain after 9 to 11 μsec of pumping, and achieved peaks of ≈ 3%/cm after the electric discharge pulse was terminated.

The sudden rise in the gain coefficient after the pulse is turned off is due to the equilibration of the rotational temperature, which can be 50 to 90° K higher than the translational temperature at the higher pumping rates. This is characteristic of a partial inversion, which is very sensitive to the rotational temperature.

It is interesting to note that in a laser cavity, nonuniformities in pumping (regions of low pumping rates) could lead to absorption coefficients that are of the same order as the gain coefficients in regions of higher pumping rates.

It is concluded from these calculations that significant optical gain can be expected when gas mixtures containing HF, H_2, and Ar are excited by an electric discharge. However, it is necessary to provide adequate electrical power input at the optimum value of E/N.

$HF/H_2/Ar = 1/10/89$

$T_o = 300°K$

$P_o = 200$ torr

$\tau_{pump} = 20$ µsec

$\frac{P_{vib}}{P_{rot}} = 1$

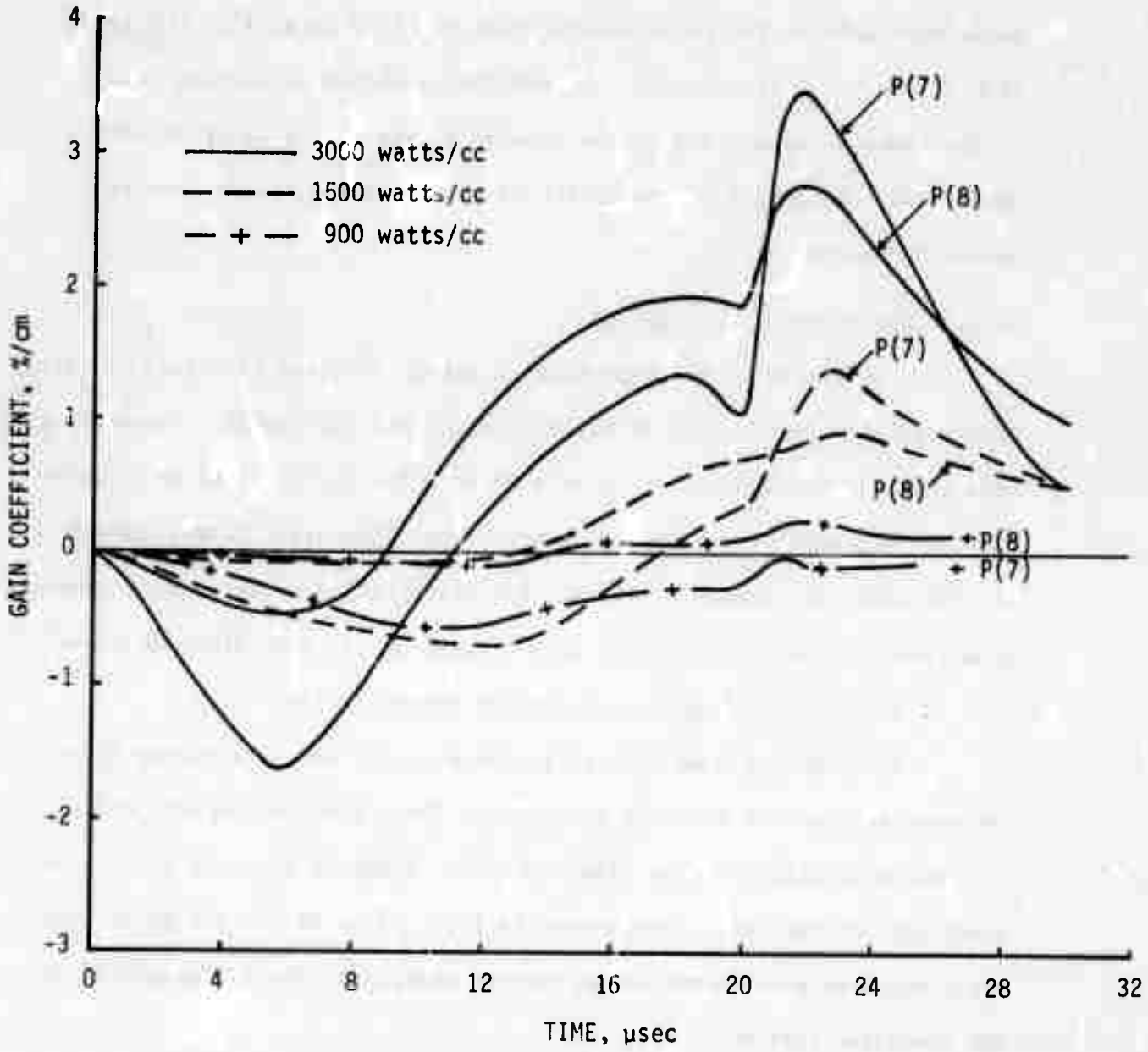

FIGURE 5. Optical Gain Coefficient for HF(v = 3 → v = 2) Transition

2.3. Experimental Observations on HF and DF

A 15 cm I.D. teflon chamber was used to make initial measurements of the characteristics of gas mixtures containing HF and DF when subjected to an electron-beam-stabilized electric discharge. The effect of electron attachment to HF was determined at a total gas pressure of 200 torr and an HF concentration ranging from 1 to 5 percent. Time dependent measurements were made of the fluorescence emission of HF as well as the absorption of the v = 1 state of HF. In addition a highly reflecting hole coupled cavity was applied to the chamber to search for laser inversion conditions. Following a description of the apparatus, these results are summarized below.

2.3.1. Experimental Arrangement

A schematic of the experimental set-up is shown in Figure 6. The teflon chamber is attached to the housing of the thermionic cathode electron beam which covers an area of 10 cm x 10 cm. The optical path is aligned with the diagonal of the resulting electrical discharge volume, providing an effective path length of 14 cm. The discharge anode is a solid aluminum plate and the discharge cathode is a 60 percent porosity aluminum screen.

a. Electron beam and electrical power supplies

The electron beam used to ionize the test gas is a 250-kv thermionic cathode, grid-pulsed electron beam with a 10-cm x 10-cm electron window of 0.04-mm thick high-strength aluminum foil. Bridging elements about 1 cm apart support the foil. The e-beam is operated at 125 to 150 kv in these experiments to provide an e-beam current density of about 5 mamps/cm^2 in the discharge region.

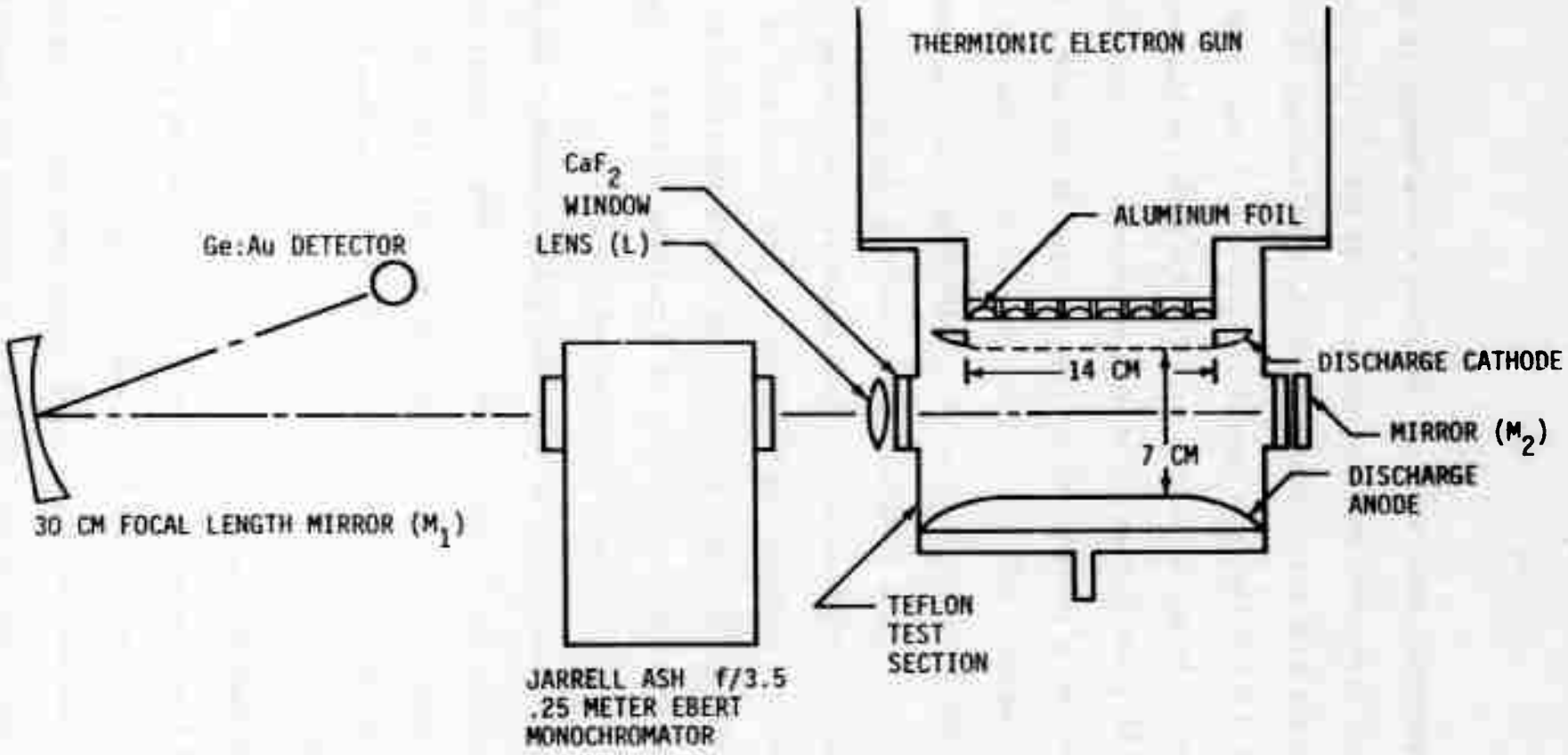

FIGURE 6. HF/DF Fluorescence Experiment

The electrical power supplies are shown schematically in Figure 7. Two heavily filtered power supplies are used, one for the electron gun, the other for the high energy discharge in the test section. During operation the 0.8 μfd discharge capacitor for the test section is held at high voltage; the gun is also at high voltage with the filaments on, and the bias adjusted so there is no e-beam current. An initiating signal first turns on the e-beam gun by changing the bias of the grid relative to the filament. After a delay of about 10 μsec to assure that gas ionization is near steady state, the discharge initiating switch is automatically energized. The discharge current occurs between a 57.5 cm^2 area aluminum screen (65 percent transmission, 0.025-mm diameter wire) and an aluminum anode; the current density is in the range of 1 to 2 amps per cm^2. The stable high pressure discharge is usually set for a time of 20 to 40 μsec. The duration of the discharge current is controlled by the electron beam current which can be adjusted from 10 to 500 μsec.

As shown in Figure 7 a 50-ohm copper sulfate resistor was used in series with a spark gap triggered capacitor (0.8 μfd) to supply current at 5 to 10 kv across a 7-cm gap in the chamber. The voltage drop across this damping resistor must be taken into account to determine the E/p across the test section.

b. Gas handling system

Figure 8 is a schematic diagram of the gas handling system. The hydrogen fluoride purification system was constructed out of monel tubing and cylinders; however, brass and steel valves were used for controls. Prior to use, the entire vacuum system for HF handling was passivated

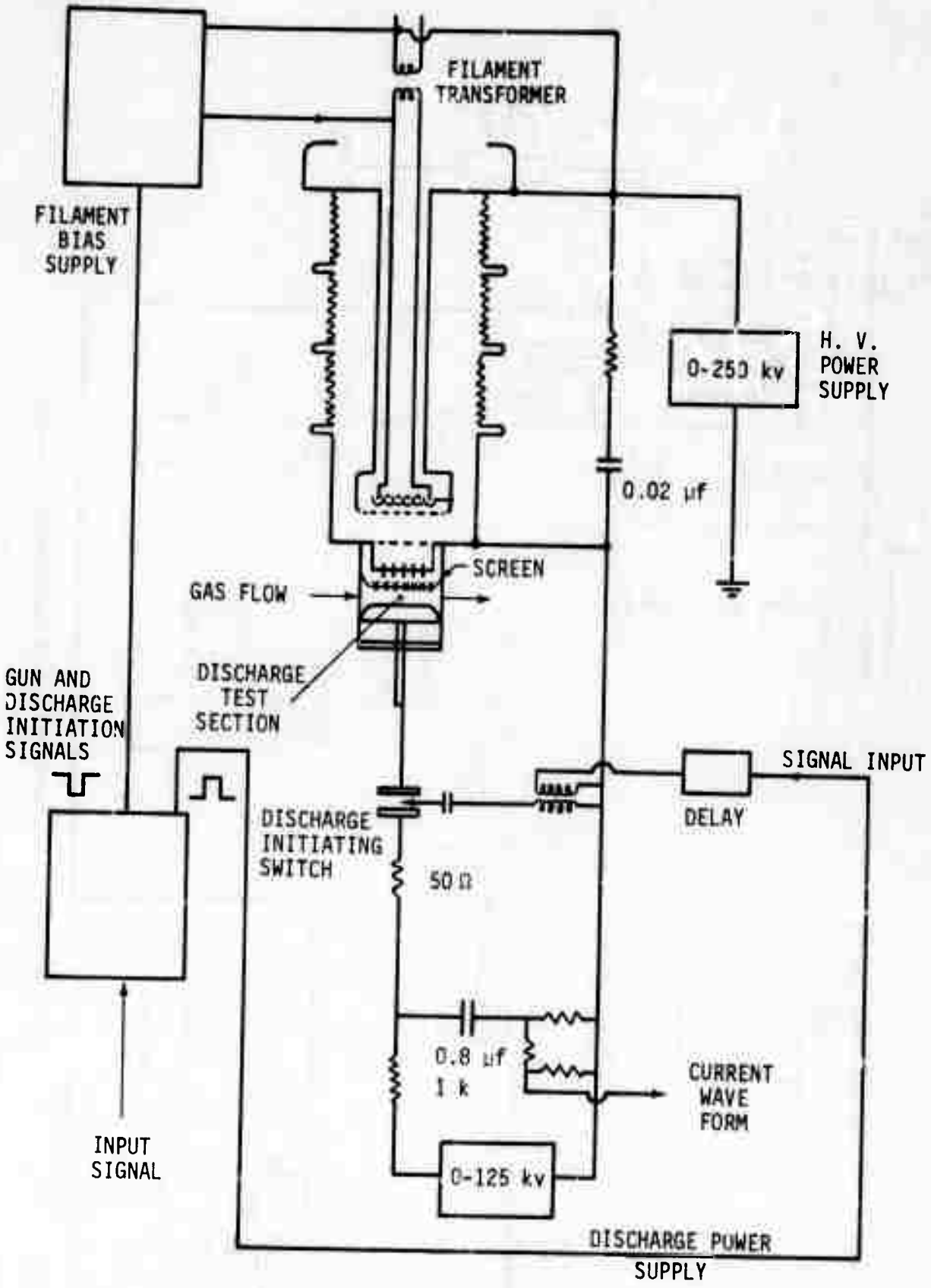

FIGURE 7. Electrical Power Supplies for the HF/DF Fluorescence Experiment

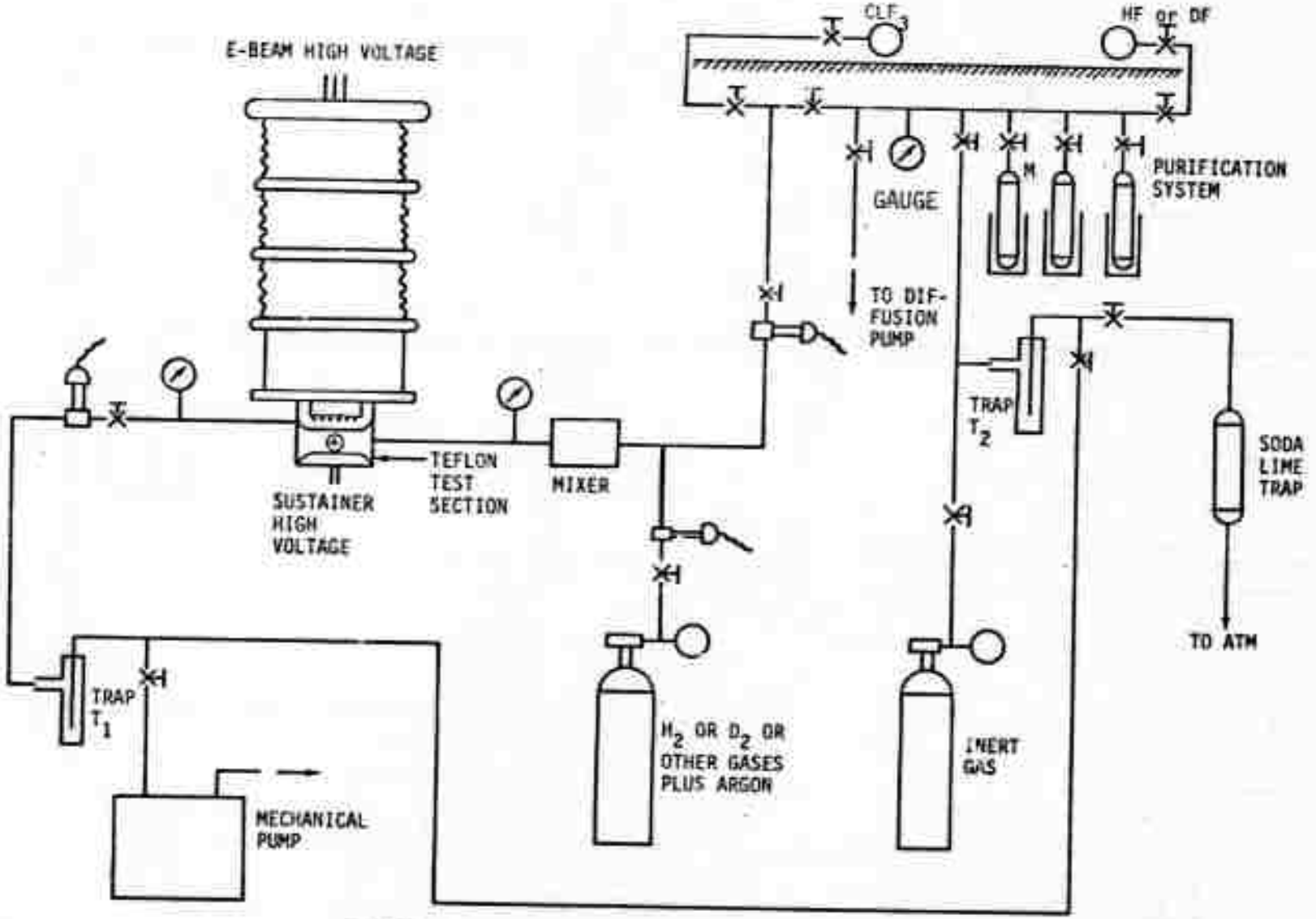

FIGURE 8. Schematic Diagram of Experimental Apparatus

using ClF_3 at 1 atmosphere pressure. A small oil diffusion pump provided a 10^{-4} torr vacuum in the entire purification section. Heating tape was wrapped around the monel tubing sections, and dewars with boiling water were used to bake out the monel storage bottles in order to speed the pump down operation. An NRC thermocouple gauge was used to monitor pressures below 1 torr, and a March Inst. Co. Type 100 M, monel gauge could be used from 10 torr up to a pressure of 30 psig.

For safety reasons, the chlorine trifluoride and hydrogen fluoride supply tanks (Matheson Gas Co.) were installed outside the building, but adjacent to the fume hood used for gas handling. Hydrogen fluoride was withdrawn from the storage tank and frozen down at liquid nitrogen temperatures into one of the monel storage tanks. All non-condensible gases were pumped away by the diffusion pump to a pressure (measured by the NRC gauge) of 10^{-3} torr. By replacing the nitrogen coolant with a dewar filled with a chloroform slurry, the HF could be brought up to its equilibrium vapor pressure (approximately 12 torr) at the chloroform melting point (-63.5° C). Liquid nitrogen was gradually mixed with the chloroform to maintain it at this temperature. Approximately 2-3 percent of the HF was discarded once it had reached 15-25 torr vapor pressure, and a bottom fraction of 5-10 percent also was not used at the completion of the distillation from chloroform slush temperature to another monel tank held at liquid nitrogen temperature. Occasionally a second distillation was performed, but no significant change in discharge behavior or light emission characteristics was observed when this was done.

Any HF gas to be disposed of was collected and frozen in a trap (T_2, Figure 8) and was then removed by warming the trap to room temperature. Dry nitrogen or helium was used to flush the HF through a soda lime reactor and was exhausted to the atmosphere. After 5 to 10 minutes of this gas purge, the trap was evacuated by the mechanical pump.

Argon (Airco 99.995 percent), hydrogen (Airco, 99.999 percent), and nitrogen (Airco, 99.99 percent) gases were used without further purification. The HF was used from the monel storage vessel at an HF pressure of 500 torr and mixed with the Ar/N_2 or Ar/H_2 gas in a flowing system. A short length of polyethylene tubing connected the monel vacuum system to the Teflon test section. The test cell filling rate was approximately 350 torr/minute. Exit gases were passed through a liquid nitrogen cooled trap (T_1), and later transferred to trap T_2 for disposal at the conclusion of an experiment.

c. Optical instrumentation

The teflon test section and optical arrangement for observing light emitted by the electron-beam stabilized discharge are shown in Figure 6. Calcium fluoride windows were used for observing emission or absorption; gold coated mirrors could be mounted internally, or Brewster angled calcium fluoride adapters could be mounted at the same ports.

Optimum collection optics for viewing light emission consisted of a flat back-up mirror (M_2), a quartz or calcium fluoride lens (L), focal length 3.5 in. - 5 in. and a monochromator placed 5 or 6 in. from the lens. A small mercury lamp placed at the rear window (M_2 removed), greatly

facilitated alignment and insured that the monochromator was properly placed. With the monochromator set for the mercury green line (5461 Å), the collection mirror (M_1) and detector (Ge:Au) were readily aligned by centering the green slit image on the 2-mm diameter detector. For several experiments a 1P28 RCA photomultiplier tube was used to observe emission in the ultraviolet-visible portion of the spectrum. For these experiments no additional mirror (M_1) was used, and the collecting lens was omitted since the photocathode size is suitable for placement immediately in front of the exit slit of the monochromator.

Amplification of the Ge:Au detector signals was accomplished by a Perry Amplifier (factor of 100 amplification) and the output displayed on a Tektronix Dual Trace Oscilloscope. The phototube utilized a cathode follower output to provide low output impedance in order to achieve adequate response time. Rise times for both detectors were approximately 1 μsec.

A Jarrell-Ash 0.25 m Ebert Spectrometer, equipped with both 6000 Å and 2.1-μ blazed gratings, was used for spectral measurements. OCLI wide-band filters were used to eliminate overlapping orders of the monochromator. Very weak emission was studied by removing the lens and monochromator, and viewing the emission using only a detector, a collection mirror (M_1), and a filter.

An HF probe laser was constructed based on a design by Ultee (Ref. 19) which uses He, SF_6 and H_2 gases to produce HF emission via the reaction of F atoms, produced in an electrical discharge, and H_2. Spectral lines are presently selected using a monochromator; however, a grating can be used in the cavity as well to force oscillation on several of the weaker

transitions. Thus far, emission on the 2 → 1 P(4) and P(5) lines has been obtained using H_2; future experiments with HBr in the probe laser will yield higher vibrational level transitions (Ref. 20).

2.3.2. Electron Attachment Measurements

The effect of electron attachment to HF was determined experimentally by measuring the electrical discharge current in the test cell as a function of HF concentration. The basic gas mixture used was 20% hydrogen, 80% argon at a pressure of 190 torr. A voltage corresponding to a value of E/N of 2×10^{-16} v - cm^2 was applied to the test chamber. The electron beam was operated at a voltage of 125 kv and a current density in the gas of 2 mamps/cm^2. The dependence of the steady-state discharge current density on HF concentration is shown in Figure 9.

A theoretical curve is also shown in Figure 9 based on the following expression for the balance between electron production and loss processes:

$$j_e \sum_i g_i N_i = \alpha N_e^2 + \beta N_e N_{HF} \qquad (13)$$

where j_e is the e-beam current density, g_i is the ion-pair production rate by collision with species i having concentration N_i, α is the dissociative recombination rate, N_e is the electron density, N_{HF} is the HF density, and β is the effective attachment rate coefficient. The theoretical curve has been fit to the data by using

$$\beta N_{HF} = 2 \alpha N_{e_o} \qquad (14)$$

at $N_{HF} = 4.4\%$. Here N_{e_o} is the value of N_e for $N_{HF} = 0$.

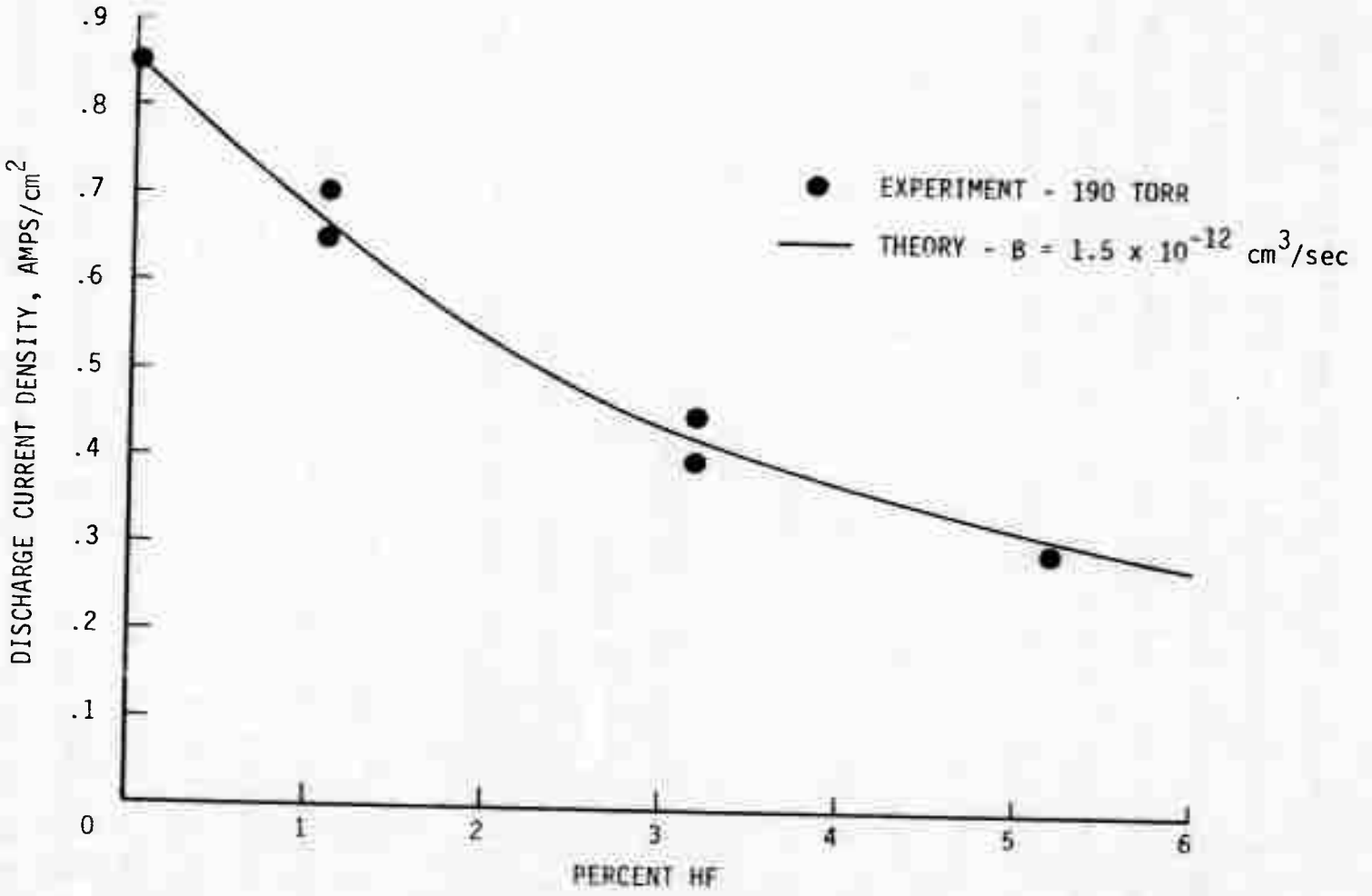

FIGURE 9. Electron Attachment by HF in 1:4 Hydrogen - Argon Mixtures

A value of g_i = 0.045 cm^2/ma was used for argon and a value of 0.005 was used for hydrogen. The electron density was determined from the measured current density and a drift velocity inferred from the work of Engelhardt and Phelps (Ref. 21) which yields $\nu_D = 3 \times 10^6$ cm/sec for these conditions. Then N_{e_o} is 1.8×10^{12} cm^{-3} and α is 1.1×10^{-7} cm^3/sec. The attachment rate inferred from the data under these conditions is $\beta = 1.5 \times 10^{-12}$ cm^3/sec.

Since the attachment to HF probably involves dissociation to $H + F^-$, the onset of the process has a threshold at about 2.2 ev. Since the electron distribution function is decreasing rapidly at this energy, it is difficult to infer a cross section from the value of β determined above. The dependence on E/N has not yet been determined. The principal conclusion from the measurement is that the attachment rate is sufficiently low to permit the use of HF at the desired concentrations with virtually no change in the electron beam current requirments due to the addition of HF.

Similar experiments were also conducted using D_2 and DF. It was found that the attachment in DF was much larger and that the discharge was much less stable, showing a much greater tendency to arc when only a small amount of DF was introduced. These effects probably arise from impurities in the DF. It was learned later that the DF supplier used a process involving H_2SO_4, and a possible impurity is SO_2. This impurity cannot be removed by the distillation process that we used in purifying the HF and DF. For this reason, the DF results will require further checking using high purity DF.

2.3.3. HF Fluorescence Measurements

Using the experimental arrangement shown in Figure 6, the fluorescence of HF in various gas mixtures was detected on an Au:Ge detector and recorded on an oscilloscope. Three such traces are shown in Figure 10. In Figure 10(a) the infrared fluorescence from 1 to 11 microns is shown; in Figure 10(b) the region from 2.3 microns and longer is shown; in Figure 10(c) the emission through a filter passing 1.47 to 1.68 microns is shown.

It is seen in Figure 10(a) that there is some infrared emission arising directly from the electron beam ionizing source. At the time the discharge is initiated there is a short emission spike followed by a nearly linear rise in intensity. At the time the electron beam is terminated and the discharge current decays a second emission spike is seen which is frequently followed by a series of such spikes. Simultaneously the background emission decays exponentially. At a time of about 50 μsec after the ionizing source is cut off, the discharge voltage leads to an arc in the test chamber for the experimental conditions shown here.

It was determined that the spikes seen in Figure 10(a) occur in the 1 to 2 micron region and probably arise from H_2 electronic state emission; this is seen in Figure 10(c) and is discussed in more detail in Section 4. With the shorter wavelength spikes blocked by a 2.3 micron long pass filter, as shown in Figure 10(b), it was determined that the emission was HF fundamental fluorescence.

(a) No Filter

(b) 2.3 Migron Long-Pass Filter

(c) 1.47 to 1.68 Micron Filter

Figure 10. Fluorescence in 1.5/10/88.5 HF-H_2-A Mixtures at E/N = 1.8×10^{-16} v-cm^2 and p = 190 Torr. Sweep speed = 20 μsec/cm. Upper trace--discharge current, 1.8 amps/cm^2 per division; middle trace--electron beam current monitor; lower trace--Au:Ge detector.

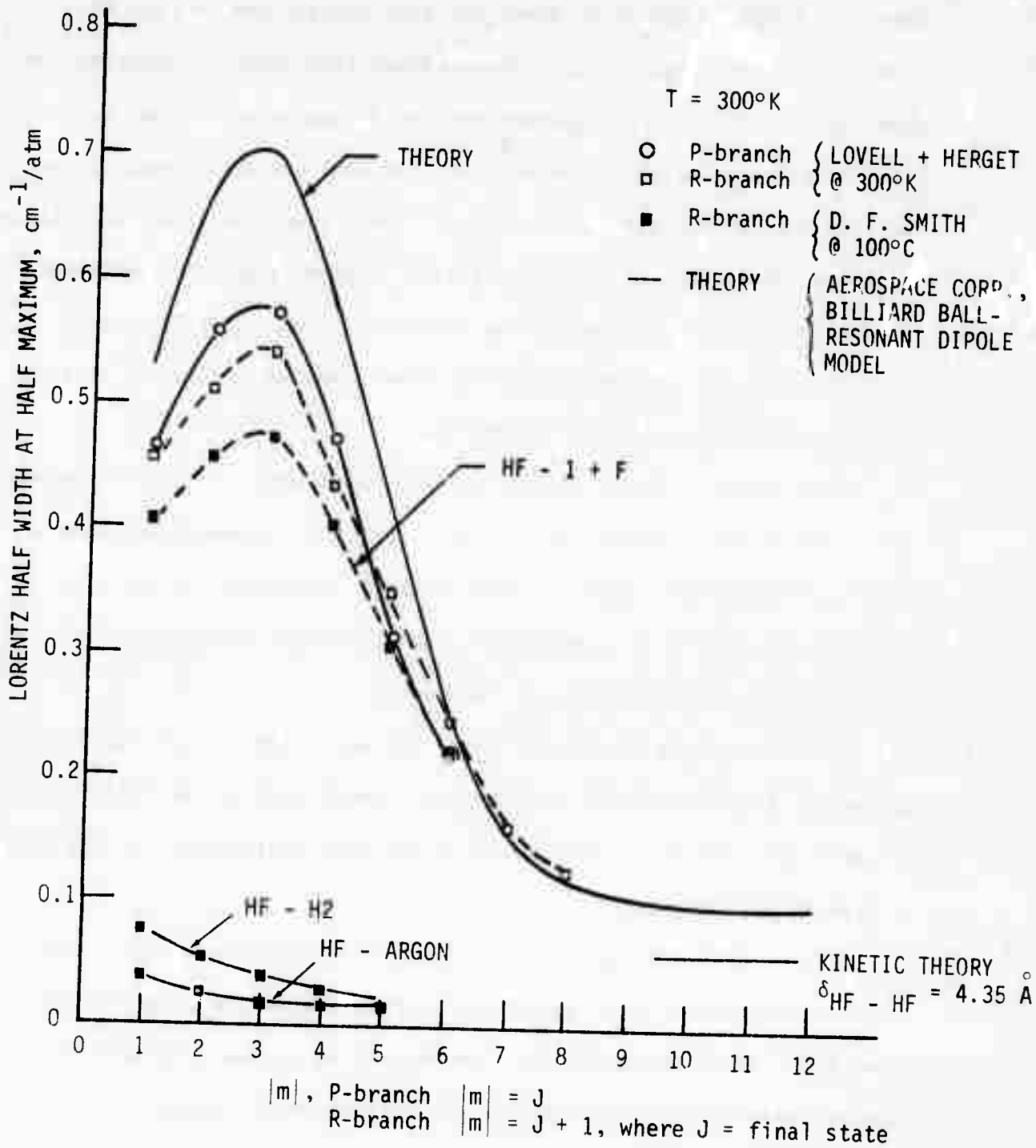

FIGURE 4. HF Lorentz Broadening

between the H_2 vibration and rotation. Results for these energy input rates are shown in Figure 5, where the gain coefficient for the HF ($v = 3 \rightarrow v = 2$) transition is plotted versus time from the onset of the input pulse. At the lower pumping rate of 900 watts/cm^3 there is no significant gain during the pulse. For the 1500 watts/cm^3 pumping rate the gain becomes positive after 14 to 17 μsec, reaching a peak of ≈ 1%/cm following termination of the input power. Highest gains were obtained for the 3000 watts/cm^3 pumping rate, which switched to positive gain after 9 to 11 μsec of pumping, and achieved peaks of ≈ 3%/cm after the electric discharge pulse was terminated.

The sudden rise in the gain coefficient after the pulse is turned off is due to the equilibration of the rotational temperature, which can be 50 to 90° K higher than the translational temperature at the higher pumping rates. This is characteristic of a partial inversion, which is very sensitive to the rotational temperature.

It is interesting to note that in a laser cavity, nonuniformities in pumping (regions of low pumping rates) could lead to absorption coefficients that are of the same order as the gain coefficients in regions of higher pumping rates.

It is concluded from these calculations that significant optical gain can be expected when gas mixtures containing HF, H_2, and Ar are excited by an electric discharge. However, it is necessary to provide adequate electrical power input at the optimum value of E/N.

$HF/H_2/Ar = 1/10/89$

$T_o = 300°K$

$P_o = 200$ torr

$\tau_{pump} = 20$ µsec

$\frac{P_{vib}}{P_{rot}} = 1$

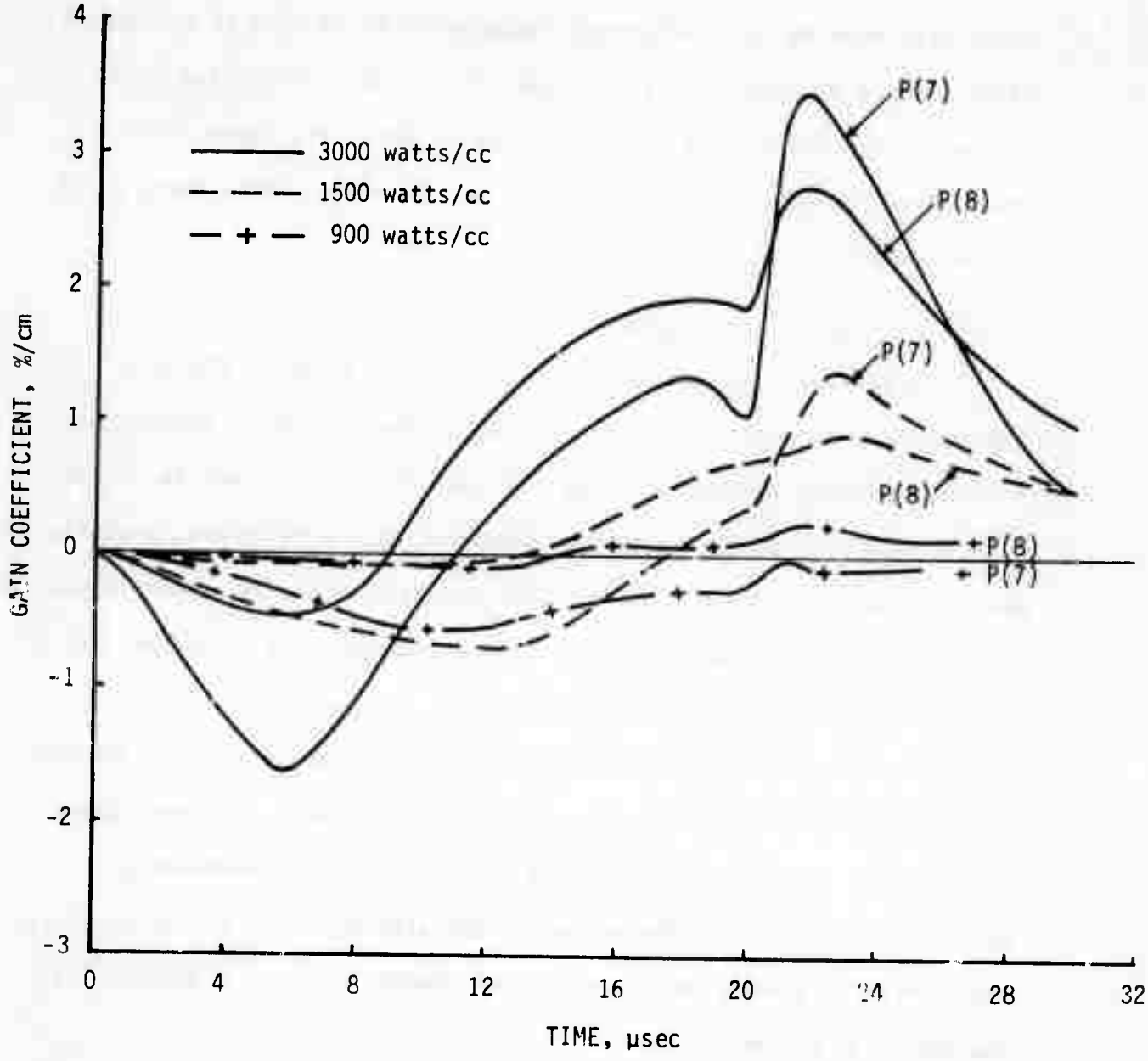

FIGURE 5. Optical Gain Coefficient for HF(v = 3 → v = 2) Transition

2.3. Experimental Observations on HF and DF

A 15 cm I.D. teflon chamber was used to make initial measurements of the characteristics of gas mixtures containing HF and DF when subjected to an electron-beam-stabilized electric discharge. The effect of electron attachment to HF was determined at a total gas pressure of 200 torr and an HF concentration ranging from 1 to 5 percent. Time dependent measurements were made of the fluorescence emission of HF as well as the absorption of the v = 1 state of HF. In addition a highly reflecting hole coupled cavity was applied to the chamber to search for laser inversion conditions. Following a description of the apparatus, these results are summarized below.

2.3.1. Experimental Arrangement

A schematic of the experimental set-up is shown in Figure 6. The teflon chamber is attached to the housing of the thermionic cathode electron beam which covers an area of 10 cm x 10 cm. The optical path is aligned with the diagonal of the resulting electrical discharge volume, providing an effective path length of 14 cm. The discharge anode is a solid aluminum plate and the discharge cathode is a 60 percent porosity aluminum screen.

a. Electron beam and electrical power supplies

The electron beam used to ionize the test gas is a 250-kv thermionic cathode, grid-pulsed electron beam with a 10-cm x 10-cm electron window of 0.04-mm thick high-strength aluminum foil. Bridging elements about 1 cm apart support the foil. The e-beam is operated at 125 to 150 kv in these experiments to provide an e-beam current density of about 5 mamps/cm^2 in the discharge region.

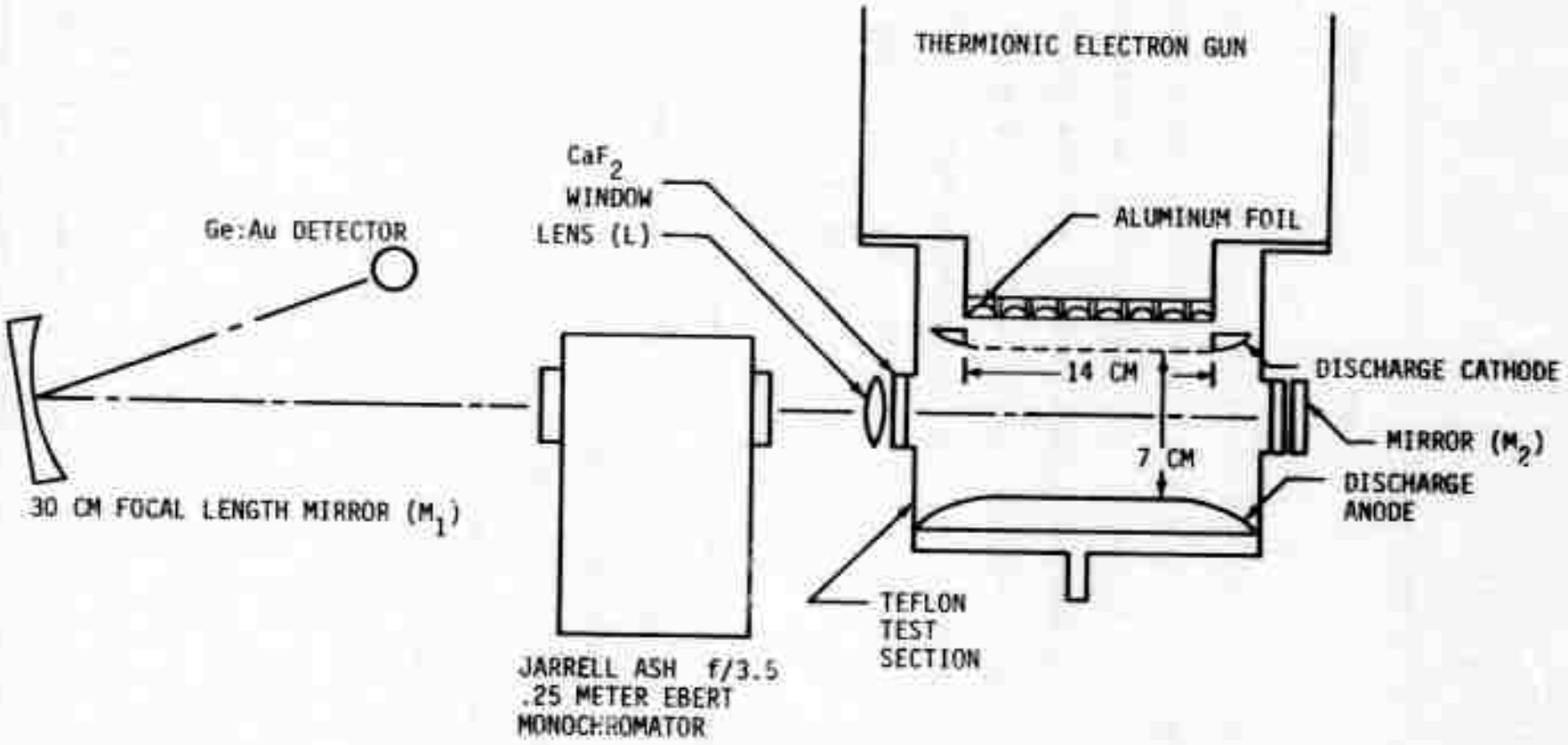

FIGURE 6. HF/DF Fluorescence Experiment

The electrical power supplies are shown schematically in Figure 7. Two heavily filtered power supplies are used, one for the electron gun, the other for the high energy discharge in the test section. During operation the 0.8 μfd discharge capacitor for the test section is held at high voltage; the gun is also at high voltage with the filaments on, and the bias adjusted so there is no e-beam current. An initiating signal first turns on the e-beam gun by changing the bias of the grid relative to the filament. After a delay of about 10 μsec to assure that gas ionization is near steady state, the discharge initiating switch is automatically energized. The discharge current occurs between a 57.5 cm^2 area aluminum screen (65 percent transmission, 0.025-mm diameter wire) and an aluminum anode; the current density is in the range of 1 to 2 amps per cm^2. The stable high pressure discharge is usually set for a time of 20 to 40 μsec. The duration of the discharge current is controlled by the electron beam current which can be adjusted from 10 to 500 μsec.

As shown in Figure 7 a 50-ohm copper sulfate resistor was used in series with a spark gap triggered capacitor (0.8 μfd) to supply current at 5 to 10 kv across a 7-cm gap in the chamber. The voltage drop across this damping resistor must be taken into account to determine the E/p across the test section.

b. Gas handling system

Figure 8 is a schematic diagram of the gas handling system. The hydrogen fluoride purification system was constructed out of monel tubing and cylinders; however, brass and steel valves were used for controls. Prior to use, the entire vacuum system for HF handling was passivated

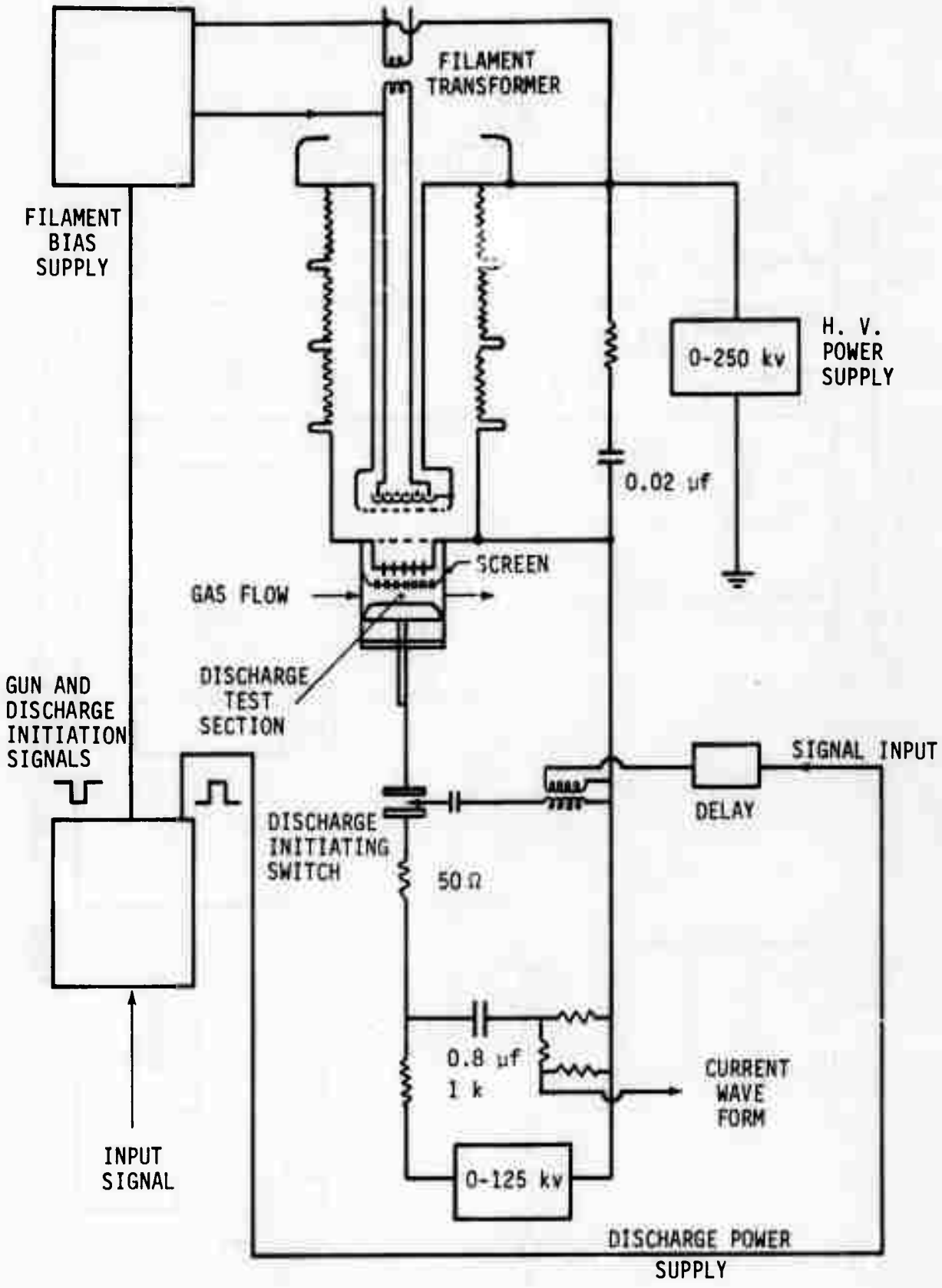

FIGURE 7. Electrical Power Supplies for the HF/DF Fluorescence Experiment

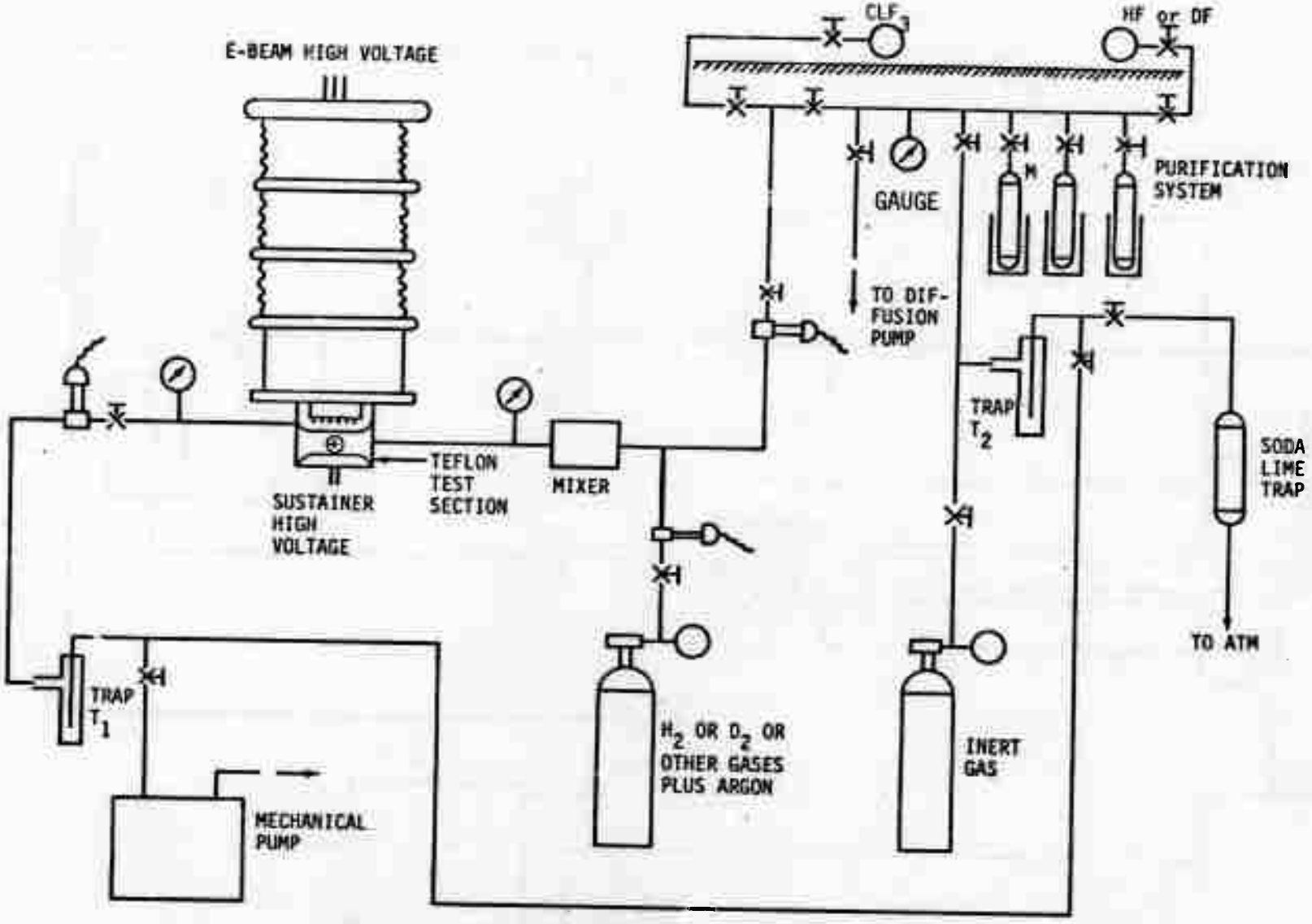

FIGURE 8. Schematic Diagram of Experimental Apparatus

using ClF_3 at 1 atmosphere pressure. A small oil diffusion pump provided a 10^{-4} torr vacuum in the entire purification section. Heating tape was wrapped around the monel tubing sections, and dewars with boiling water were used to bake out the monel storage bottles in order to speed the pump down operation. An NRC thermocouple gauge was used to monitor pressures below 1 torr, and a March Inst. Co. Type 100 M, monel gauge could be used from 10 torr up to a pressure of 30 psig.

For safety reasons, the chlorine trifluoride and hydrogen fluoride supply tanks (Matheson Gas Co.) were installed outside the building, but adjacent to the fume hood used for gas handling. Hydrogen fluoride was withdrawn from the storage tank and frozen down at liquid nitrogen temperatures into one of the monel storage tanks. All non-condensible gases were pumped away by the diffusion pump to a pressure (measured by the NRC gauge) of 10^{-3} torr. By replacing the nitrogen coolant with a dewar filled with a chloroform slurry, the HF could be brought up to its equilibrium vapor pressure (approximately 12 torr) at the chloroform melting point (-63.5° C). Liquid nitrogen was gradually mixed with the chloroform to maintain it at this temperature. Approximately 2-3 percent of the HF was discarded once it had reached 15-25 torr vapor pressure, and a bottom fraction of 5-10 percent also was not used at the completion of the distillation from chloroform slush temperature to another monel tank held at liquid nitrogen temperature. Occasionally a second distillation was performed, but no significant change in discharge behavior or light emission characteristics was observed when this was done.

Any HF gas to be disposed of was collected and frozen in a trap (T_2, Figure 8) and was then removed by warming the trap to room temperature. Dry nitrogen or helium was used to flush the HF through a soda lime reactor and was exhausted to the atmosphere. After 5 to 10 minutes of this gas purge, the trap was evacuated by the mechanical pump.

Argon (Airco 99.995 percent), hydrogen (Airco, 99.999 percent), and nitrogen (Airco, 99.99 percent) gases were used without further purification. The HF was used from the monel storage vessel at an HF pressure of 500 torr and mixed with the Ar/N_2 or Ar/H_2 gas in a flowing system. A short length of polyethylene tubing connected the monel vacuum system to the Teflon test section. The test cell filling rate was approximately 350 torr/minute. Exit gases were passed through a liquid nitrogen cooled trap (T_1), and later transferred to trap T_2 for disposal at the conclusion of an experiment.

c. Optical instrumentation

The teflon test section and optical arrangement for observing light emitted by the electron-beam stabilized discharge are shown in Figure 6. Calcium fluoride windows were used for observing emission or absorption; gold coated mirrors could be mounted internally, or Brewster angled calcium fluoride adapters could be mounted at the same ports.

Optimum collection optics for viewing light emission consisted of a flat back-up mirror (M_2), a quartz or calcium fluoride lens (L), focal length 3.5 in. - 5 in. and a monochromator placed 5 or 6 in. from the lens. A small mercury lamp placed at the rear window (M_2 removed), greatly

facilitated alignment and insured that the monochromator was properly placed. With the monochromator set for the mercury green line (5461 Å), the collection mirror (M_1) and detector (Ge:Au) were readily aligned by centering the green slit image on the 2-mm diameter detector. For several experiments a 1P28 RCA photomultiplier tube was used to observe emission in the ultraviolet-visible portion of the spectrum. For these experiments no additional mirror (M_1) was used, and the collecting lens was omitted since the photocathode size is suitable for placement immediately in front of the exit slit of the monochromator.

Amplification of the Ge:Au detector signals was accomplished by a Perry Amplifier (factor of 100 amplification) and the output displayed on a Tektronix Dual Trace Oscilloscope. The phototube utilized a cathode follower output to provide low output impedance in order to achieve adequate response time. Rise times for both detectors were approximately 1 μsec.

A Jarrell-Ash 0.25 m Ebert Spectrometer, equipped with both 6000 Å and 2.1-μ blazed gratings, was used for spectral measurements. OCLI wide-band filters were used to eliminate overlapping orders of the monochromator. Very weak emission was studied by removing the lens and monochromator, and viewing the emission using only a detector, a collection mirror (M_1), and a filter.

An HF probe laser was constructed based on a design by Ultee (Ref. 19) which uses He, SF_6 and H_2 gases to produce HF emission via the reaction of F atoms, produced in an electrical discharge, and H_2. Spectral lines are presently selected using a monochromator; however, a grating can be used in the cavity as well to force oscillation on several of the weaker

transitions. Thus far, emission on the 2 → 1 P(4) and P(5) lines has been obtained using H_2; future experiments with HBr in the probe laser will yield higher vibrational level transitions (Ref. 20).

2.3.2. Electron Attachment Measurements

The effect of electron attachment to HF was determined experimentally by measuring the electrical discharge current in the test cell as a function of HF concentration. The basic gas mixture used was 20% hydrogen, 80% argon at a pressure of 190 torr. A voltage corresponding to a value of E/N of 2×10^{-16} v - cm^2 was applied to the test chamber. The electron beam was operated at a voltage of 125 kv and a current density in the gas of 2 mamps/cm^2. The dependence of the steady-state discharge current density on HF concentration is shown in Figure 9.

A theoretical curve is also shown in Figure 9 based on the following expression for the balance between electron production and loss processes:

$$j_e \sum_i g_i N_i = \alpha N_e^2 + \beta N_e N_{HF} \qquad (13)$$

where j_e is the e-beam current density, g_i is the ion-pair production rate by collision with species i having concentration N_i, α is the dissociative recombination rate, N_e is the electron density, N_{HF} is the HF density, and β is the effective attachment rate coefficient. The theoretical curve has been fit to the data by using

$$\beta N_{HF} = 2 \alpha N_{e_o} \qquad (14)$$

at $N_{HF} = 4.4\%$. Here N_{e_o} is the value of N_e for $N_{HF} = 0$.

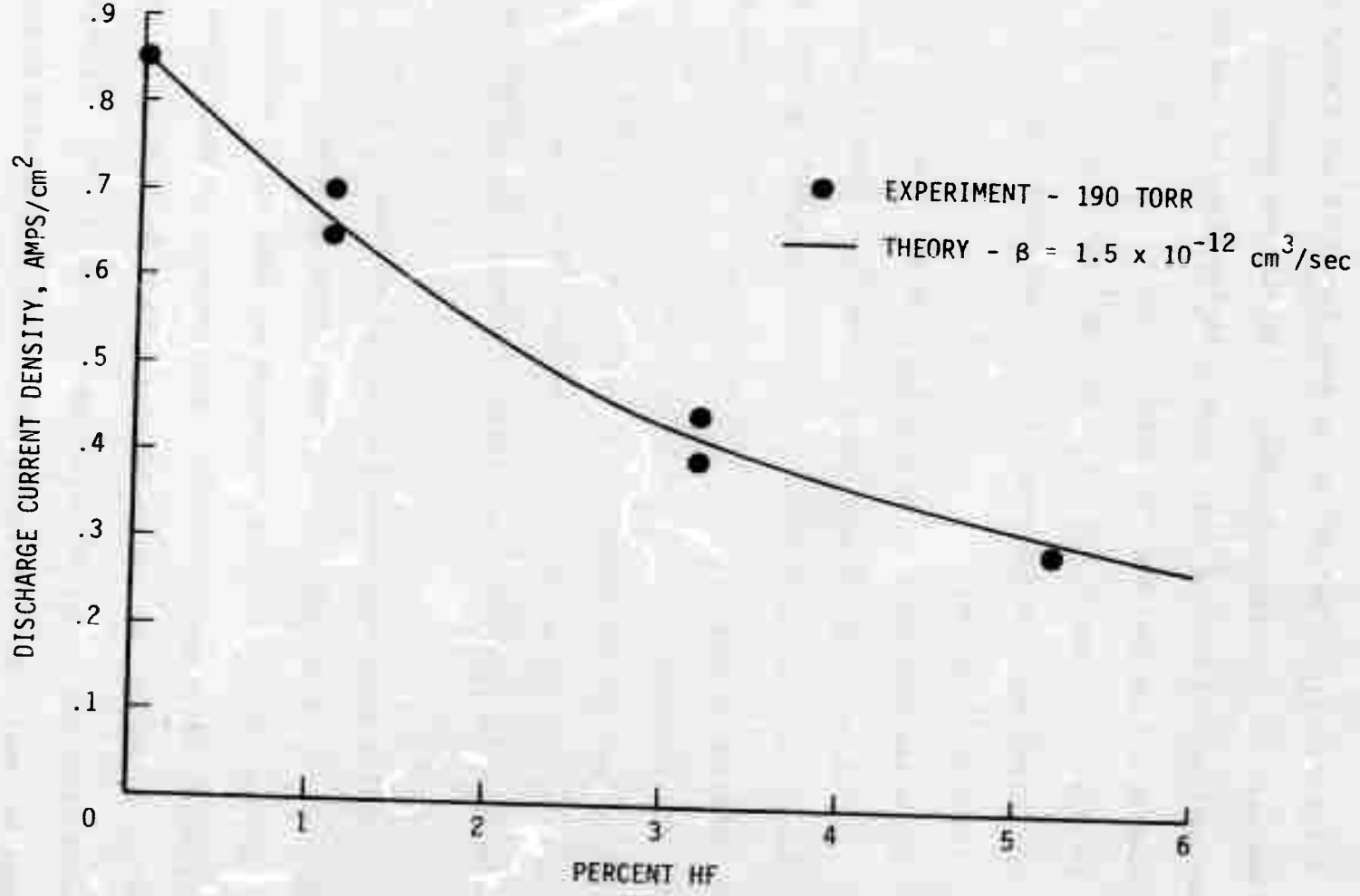

FIGURE 9. Electron Attachment by HF in 1:4 Hydrogen - Argon Mixtures

A value of $g_i = 0.045$ cm^2/ma was used for argon and a value of 0.005 was used for hydrogen. The electron density was determined from the measured current density and a drift velocity inferred from the work of Engelhardt and Phelps (Ref. 21) which yields $\nu_D = 3 \times 10^6$ cm/sec for these conditions. Then N_{e_o} is 1.8×10^{12} cm^{-3} and α is 1.1×10^{-7} cm^3/sec. The attachment rate inferred from the data under these conditions is $\beta = 1.5 \times 10^{-12}$ cm^3/sec.

Since the attachment to HF probably involves dissociation to $H + F^-$, the onset of the process has a threshold at about 2.2 ev. Since the electron distribution function is decreasing rapidly at this energy, it is difficult to infer a cross section from the value of β determined above. The dependence on E/N has not yet been determined. The principal conclusion from the measurement is that the attachment rate is sufficiently low to permit the use of HF at the desired concentrations with virtually no change in the electron beam current requirments due to the addition of HF.

Similar experiments were also conducted using D_2 and DF. It was found that the attachment in DF was much larger and that the discharge was much less stable, showing a much greater tendency to arc when only a small amount of DF was introduced. These effects probably arise from impurities in the DF. It was learned later that the DF supplier used a process involving H_2SO_4, and a possible impurity is SO_2. This impurity cannot be removed by the distillation process that we used in purifying the HF and DF. For this reason, the DF results will require further checking using high purity DF.

2.3.3. HF Fluorescence Measurements

Using the experimental arrangement shown in Figure 6, the fluorescence of HF in various gas mixtures was detected on an Au:Ge detector and recorded on an oscilloscope. Three such traces are shown in Figure 10. In Figure 10(a) the infrared fluorescence from 1 to 11 microns is shown; in Figure 10(b) the region from 2.3 microns and longer is shown; in Figure 10(c) the emission through a filter passing 1.47 to 1.68 microns is shown.

It is seen in Figure 10(a) that there is some infrared emission arising directly from the electron beam ionizing source. At the time the discharge is initiated there is a short emission spike followed by a nearly linear rise in intensity. At the time the electron beam is terminated and the discharge current decays a second emission spike is seen which is frequently followed by a series of such spikes. Simultaneously the background emission decays exponentially. At a time of about 50 μsec after the ionizing source is cut off, the discharge voltage leads to an arc in the test chamber for the experimental conditions shown here.

It was determined that the spikes seen in Figure 10(a) occur in the 1 to 2 micron region and probably arise from H_2 electronic state emission; this is seen in Figure 10(c) and is discussed in more detail in Section 4. With the shorter wavelength spikes blocked by a 2.3 micron long pass filter, as shown in Figure 10(b), it was determined that the emission was HF fundamental fluorescence.

(a) No Filter

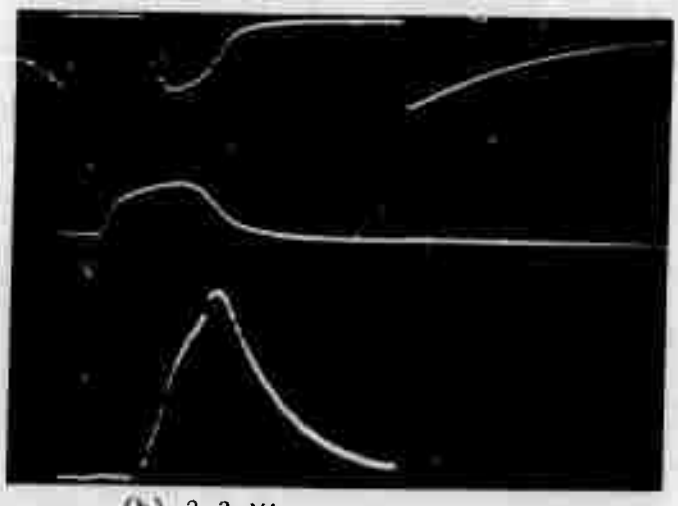

(b) 2.3 Migron Long-Pass Filter

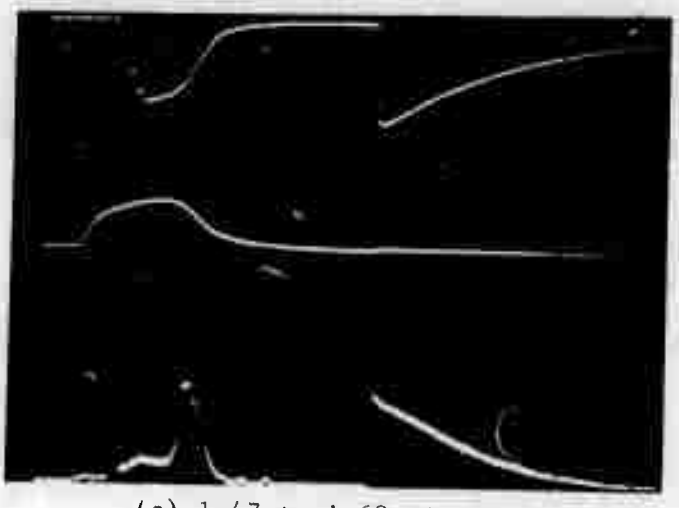

(c) 1.47 to 1.68 Micron Filter

Figure 10. Fluorescence in 1.5/10/88.5 HF-H_2-A Mixtures at E/N = 1.8 x 10^{-16} v-cm^2 and p = 190 Torr. Sweep speed = 20 μsec/cm. Upper trace--discharge current, 1.8 amps/cm^2 per division; middle trace--electron beam current monitor; lower trace--Au:Ge detector.

The 2.3 to 3 micron emission is seen to rise nearly linearly until the discharge is terminated. The subsequent decay of the HF fluorescence emission was plotted on semi-log coordinates and was well represanted by a single exponential. The observed decay times for several gas mixtures are shown in Figure 11. Note that the data were taken at 190 Torr and are referred to 1 atm pressure in Figure 11 using binary scaling. Each data point represents several experiments which were quite reproducible at a given condition. The principal uncertainty in the data is the percent HF actually present in the gas mixture. The uncertainty was generally less than 25 percent of the HF concentration used.

Also shown in Figure 11 is an approximate theoretical calculation of the fluorescent decay of HF(v = 1) assuming v = 2 of HF and H_2 are not significantly populated. This was calculated assuming V-V equilibration between H_2 and HF, which leads to the following expression at 300° K:

$$\tau = \frac{1 + 2.6(N_{HF}/N_{H_2})}{p_{HF}(\text{torr})\ [k_1 + 2.6\ k_2 + 2.6\ k_3(N_{HF}/N_{H_2}) + k_4(N_{H_2}/N_{HF})} \qquad (15)$$

where p_{HF} is the partial pressure of HF. The factor 2.6 is exp(288/T) which arises due to the vibrational energy difference between H_2 and HF. The rate constants used here in $(\mu\text{sec-torr})^{-1}$ are H_2 decay by HF (or vice versa), $k_1 + 2.6\ k_2 = 1.6 \times 10^{-3}$ (private communication from J. Bott); HF self V-T decay, $k_3 = 0.08$; and H_2 self V-T decay, $k_4 = 1 \times 10^{-6}$. It is seen that the experimental data differ from the expected values by less than a factor of 1.5. This may be due to some contribution from V = 2 emission or to a systematic error in the HF concentration. The fluorescence

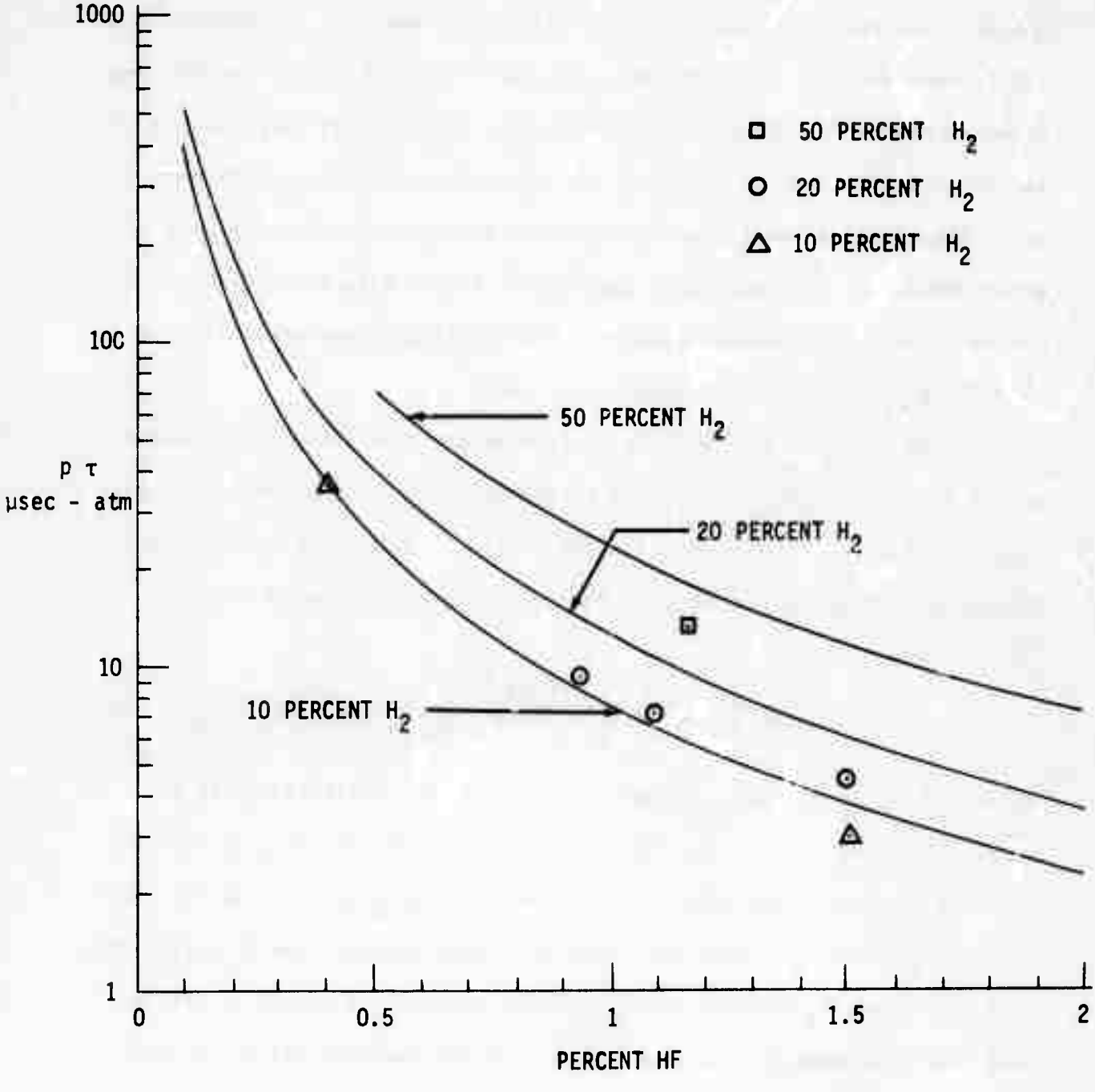

FIGURE 11. Combined V - T Decay Time for $HF/H_2/Ar$ Mixtures at 300° K

signal to noise ratio using the monochromator was not large enough to permit a single vibration-rotation line to be observed. More accurate determination of the decay time will be carried out using the probe laser to measure absorption on individual lines.

The principal conclusion from these observations is that the decay time is sufficiently long to permit effective vibrational excitation in a pulse duration of about 20 μsec provided the HF concentration is 0.5 to 1.0 percent and the H_2 concentration is of the order of 20 percent. The time scale is increased directly as the pressure is decreased below 1 atm.

The effect of N_2 rather than H_2 on HF fluorescence was also studied. It was found that electrical discharge excitation of emission at 2.3 microns and beyond was at least 10 times smaller with 10 percent N_2 in Ar than it was with 10 percent H_2 in Ar. Since the electric discharge excites N_2 vibration very effectively (more readily than H_2 is excited), we are led to the conclusion that the probability of vibrational transfer by a 2 quantum transition in N_2 to excite v = 1 of HF must be very small and will not provide a useful approach to electrical discharge excitation of HF. The same result was also observed using gas mixtures of 10 percent CO in Ar.

2.3.4. HF Absorption Measurements

The fluorescence decay measurements described in the previous Section 2.3.3 indicated that the V-T decay of HF-H_2-Ar mixtures is sufficiently long to permit the possibility of achieving a laser inversion. However, the actual population of the excited vibrational states was not

determined by the fluorescence measurements. Thus the effectiveness of electric discharge excitation of H_2 and V-V transfer to HF was not evaluated in those experiments. To obtain more quantitative data on the excited state populations the short pulse, chemical probe laser described in Section 2.3.1(c) was used in conjunction with the test cell and monochromator shown in Figure 6 to measure the absorption coefficient on selected lines.

The probe laser was operated on the P(5), P(7), and P(8) lines of the $V = 2 \rightarrow 1$ transition of HF. Thus the measured absorption was due to the $V = 1$ state of HF. Since the probe laser pulse duration was only about 1 μsec it was necessary to use a number of pulses to obtain a time history of the absorption throughout 1 pulse. This required that both the probe laser and the test gas discharge characteristics be reproducible. This was checked regularly and found to be acceptable, causing an error in I/I_o of less than ± 10 percent. The test cell geometry was altered somewhat to provide better electron beam uniformity. In this configuration an optical path of 10 cm was used.

The results for the P(5) line of the $V=2\rightarrow1$ transition in discharges into a 1/10/89 HF-H_2-Ar mixture are shown in Figure 12. Also shown are theoretical curves based on the assumption that 50 percent of the discharge energy goes into vibration and 50 percent into rotation. The V-V and V-T rates used here are those given in Table II-2. The abrupt decrease in absorption when the pulse is terminated arises from rapid rotational relaxation. It is seen that the agreement between theory and experiment is satisfactory, indicating that a significant fraction of the electrical

discharge power is transferred to vibration of H_2 and HF and that the theoretical model is not grossly in error. However, the specific dependence of absorption coefficient on power input is not yet well reproduced.

A further check on the energy partition and the theoretical model is obtained by comparing theory and experiment on the P(7) and P(8) lines of the V = 2 → 1 transition. The theoretical predictions are shown in Figure 12. Here the experimentally observed values of the transmitted probe laser intensity were very close to the original signal. Thus the change in signal level due to absorption (or gain) was not significantly more than the change due to the repeatability of the probe laser. Thus it was found that, under conditions for which the P(5) transmission was 0.2 to 0.4, the P(7) and P(8) transmission was 0.9 ± 0.1. This is in agreement with the theoretical curves shown in Figure 12 within the accuracy of the measurement.

The low absorption on the P(7) line indicates that the rotational excitation and heating of the gas is not larger than was assumed in the theoretical model; the high absorption on the P(5) line indicates that the vibrational excitation is appreciable.

For these experimental conditions the theory predicts that the 3 → 2 transition reaches a partial inversion on the P(7) and P(8) lines, but the gain is not very large and could not readily be measured using the probe laser. The results indicate that a high-Q-cavity may yield laser oscillation.

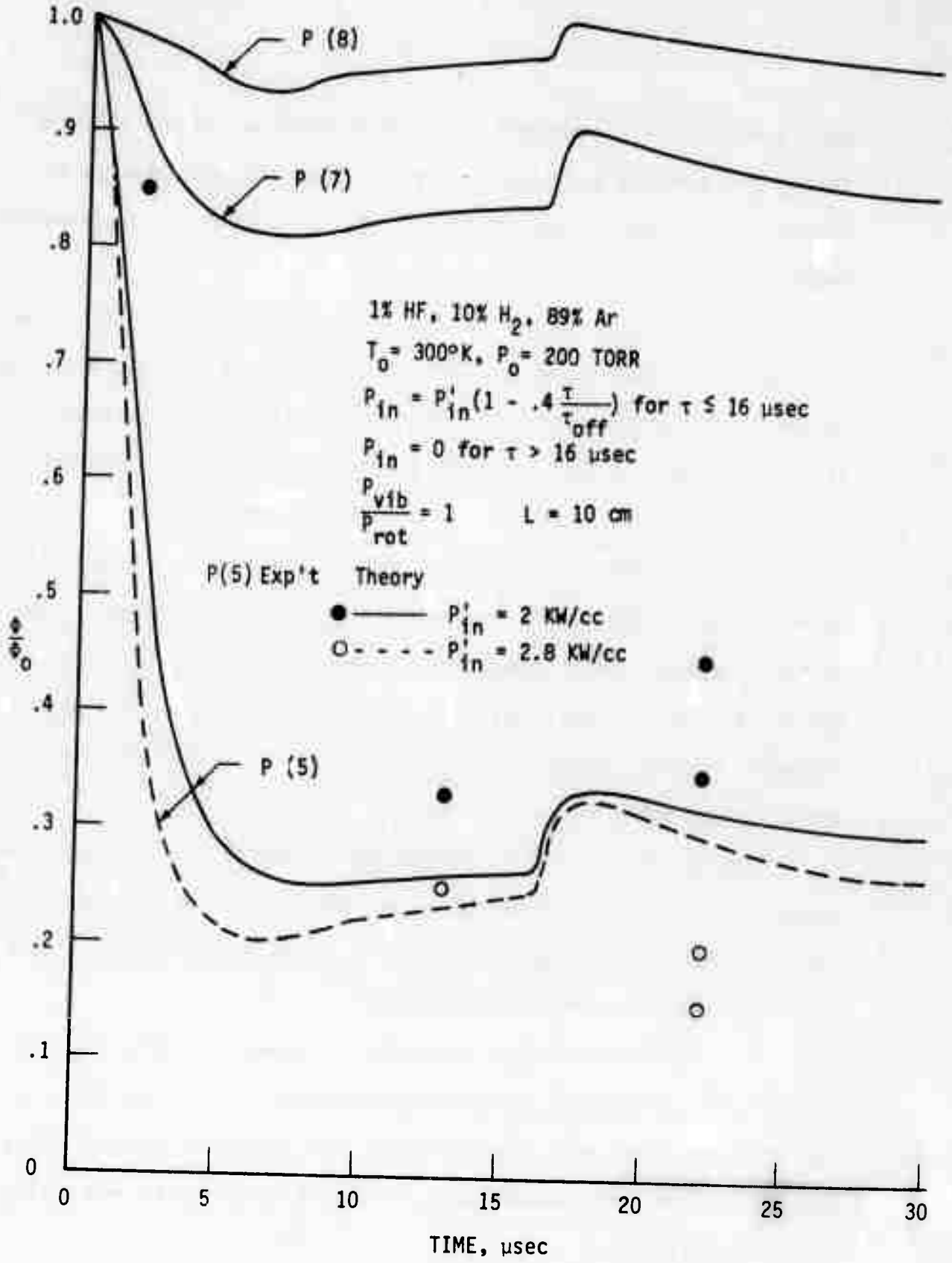

FIGURE 12. Absorption on HF (v = 1) Lines

2.3.5. Laser Cavity Measurements

The fluorescence decay and the probe laser absorption measurements indicate that the theoretical model contains many of the basic elements of the electrical discharge excitation of the vibrational energy of HF-H_2-Ar mixtures. The detailed V-T and V-V rates of the upper levels of HF remain unknown, however, and will have an important effect on the performance of this approach as a laser. To test the laser possibilities, two cavities were applied to the test cell, and the Au:Ge detector was used to search for conditions that would produce laser output.

One cavity was based on internal gold-coated glass mirrors with a hole coupled output. It was subsequently found that the substrate was attacked by HF, which caused separation of the coating and led to mottled surface and degraded the optical quality of the cavity. The second cavity was based on external gold-coated mirrors with Brewster angle CaF_2 windows on the test cell. The Au:Ge detector viewed specularly reflected light from one of the CaF_2 windows in the cavity. The Q of the cavity was checked by replacing the CaF_2 windows by KCl windows and operating the system as a CO_2 laser. The threshold gain of this cavity for CO_2 was estimated from the electrical discharge characteristics and a CO_2 kinetics program to be about 0.01 cm^{-1}.

No laser output was observed on HF. It was subsequently recognized that the values of E/p being used were too high. Thus the high energy input and the correspondingly high absorption on the P(5) V = 2 → 1 transition noted in Section 2.3.4 were achieved at values of E/N that were so

high that significant dissociation of H_2 could occur. To achieve the necessary power input at lower E/N, a higher electron beam current is required. In addition, a longer optical path is needed in order to lower the threshold gain required in the system. These changes are being made and will be tested during the next reporting period.

2.4. Summary of Results

It is concluded from the theoretical and small scale experimental studies of electrical discharges in HF-H_2-Ar and DF-D_2-Ar gas mixtures that the possibility of producing useful lasers appears feasible. In particular, it has been found that

1. Electron attachment to HF is sufficiently slow that it will not cause serious difficulty.
2. Externally stabilized electric discharges are effective in exciting vibration of H_2 and HF.
3. The VT decay rate of HF-H_2-Ar mixtures is slow enough to permit reasonable pulse durations at pressures up to 1 atm.
4. To verify HF and DF laser action by this mechanism, it will be necessary to utilize higher electron density and a longer optical path as well as more highly purified DF. These changes are in progress.

SECTION III

HIGH PRESSURE, LONG DURATION PULSED LASER TECHNOLOGY

The electron beam stabilized electric discharge has permitted efficient CO_2 laser operation at pressures up to 1 atm. This pressure level provides a pulsed CO_2 laser output energy of about 50 j/liter. In addition a pulse time duration of no more than 20 to 30 μsec is used in order to assure that acoustic wave motion cannot cause severe optical degradation of the laser medium.

The extrapolation of this performance capability to large energy leads to very large volume devices. This can be alleviated in part by operating at higher gas pressure. However at large laser energy, nonlinear propagation effects arise at the high intensities associated with short pulse duration. This can be alleviated in part by designing the laser to permit long pulse duration operation while retaining good optical quality of the medium.

For these reasons, a small scale experimental study of the possibilities of operating at high pressures and long pulse durations was carried out by P.I. and MSNW. The immediate goal of the study was to identify any unexpected obstacles and to establish criteria that would be helpful in the design of a 5 to 10 atm, 20 liter device. The following principal problem areas were addressed:

1. Electric discharge current density at high pressure.
2. Arc formation at high pressure
3. Optical gain at high pressure

4. Optical distortion due to

   a. Cathode waves

   b. Side wall shadowing of the electron beam

These effects are discussed below.

3.1. Experimental Arrangement

The electron beam and electrical power supplies used here have been described in Section 2.3.1. The electron beam for these experiments was operated at 150 kv and at a current density through a 0.025mm titanium foil of 2 ma/cm^2. A high pressure lucite test chamber was used with aluminum electrodes that provided a 10-cm x 10-cm x 10-cm discharge volume. Laser gas mixtures containing He-N_2-CO_2 were introduced at one side of the chamber and exhausted at the other side. It was found that a steady flow was necessary to achieve full discharge current; there was apparently an impurity from the walls that caused electron loss in the gas if the flow was interrupted.

Electrical discharge properties were measured using conventional voltage and current monitoring instrumentation. Optical gain was determined along a 10-cm path using a diffraction limited CW CO_2 probe laser operating on the P(20) line. A mechanical chopper was used to determine the laser intensity at the time of the measurement. Optical disturbances in the medium were measured using a Q-switched, double-pulse, ruby laser holographic interferometer described previously in Reference 22. The test cell was designed with 10-cm square optical glass windows on opposite sides.

3.2. Electrical Discharge Characteristics

A series of tests was made to determine the limitations on electrical energy input at high pressures. For this study, the discharge electrode spacing was reduced to 5 cm in order to minimize the effects of electron-beam scattering. The pulse duration was set at 25 μsec. The maximum voltage that could be applied with no arcing during the pulse is shown in Figure 13 for a 3/2/1 He-N_2-CO_2 gas mixture. Also shown are the current density and the electrical energy input at the maximum voltage.

It is seen that the maximum E/p decreases significantly as the pressure is increased. This may be associated with local breakdown in regions of high electric field, or it may be due to impurities in the gas mixture, or it may arise from the intrinsic arc formation characteristics of the gas or the gas-solid wall interface. The high electric field effect is accentuated by the higher electron beam scattering that occurs at high gas pressure.

For a fixed value of E/p, the current density increased directly as $p^{0.5}$ between 1 and 3 atm indicating that dissociative recombination remains dominant. The recombination rate inferred from the decay of the discharge current when the electron beam was interrupted was 10^{-7} cm^{-3} at 3 atm. At higher pressures, however, the current density decreased at fixed E/p. This may be caused by electron beam scattering at the higher pressures which reduced the ionization level near the discharge anode, or it may be caused by electron attachment to impurities which is accentuated at high pressure. It may also be due to three body recombination processes involving the neutral molecule as the third body. To obtain design data above

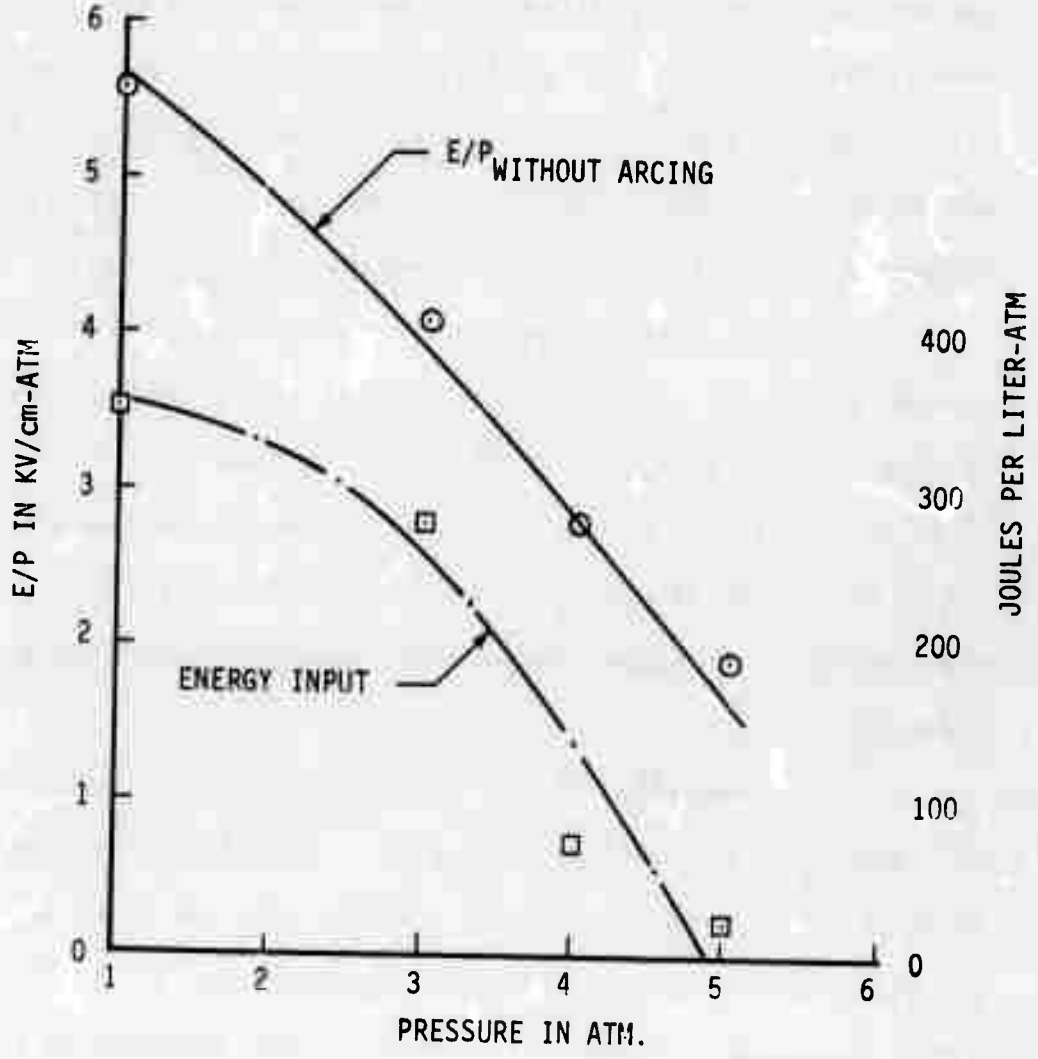

FIGURE 13. Effect of Pressure on Discharge Parameters

3 atm, further study of this problem is needed in a very clean, very uniform electrode geometry, using higher electron beam voltages.

3.3. Optical Gain at High Pressure

The kinetics of CO_2 are by now quite well established and performance predictions can be made at high pressure with some confidence. To verify this experimentally a series of tests was carried out to measure CO_2 gain at 1 to 3 atm. A pulse duration of 25 μsec was used. Typical results of gain vs time are compared with theory (Ref. 23) in Figure 14. Good agreement is apparent. The reduced gain at the higher pressure is due to the faster VT decay of CO_2 vibrational energy. This effect is illustrated more clearly in Figure 15. At high pressure the gain was found to depend strongly on the discharge power input but very little on the value of E/p. All of these effects are in accord with theoretical predictions.

Efficient power extraction can best be achieved by using lower concentrations of CO_2 as the pressure is increased, thereby reducing the decay rate of CO_2. This has been applied to shock-tube-driven gasdynamic laser technology and has proved very effective in permitting high pressure operation (Reference 24). Experiments using 60 He, 30 N_2, 10 CO_2 and 75 He, 20 N_2, 5 CO_2 at 1 to 2 atm pressure showed that the optical gain reached was affected very little by the gas mixture and the pressure and discharge energy dependence was essentially the same as that shown in Figure 15.

It is concluded, from these small scale tests in CO_2 mixtures up to 3 atm, that the electrical discharge pumping, the VV and VT rates, the optical gain, and the saturation intensity are well described by current

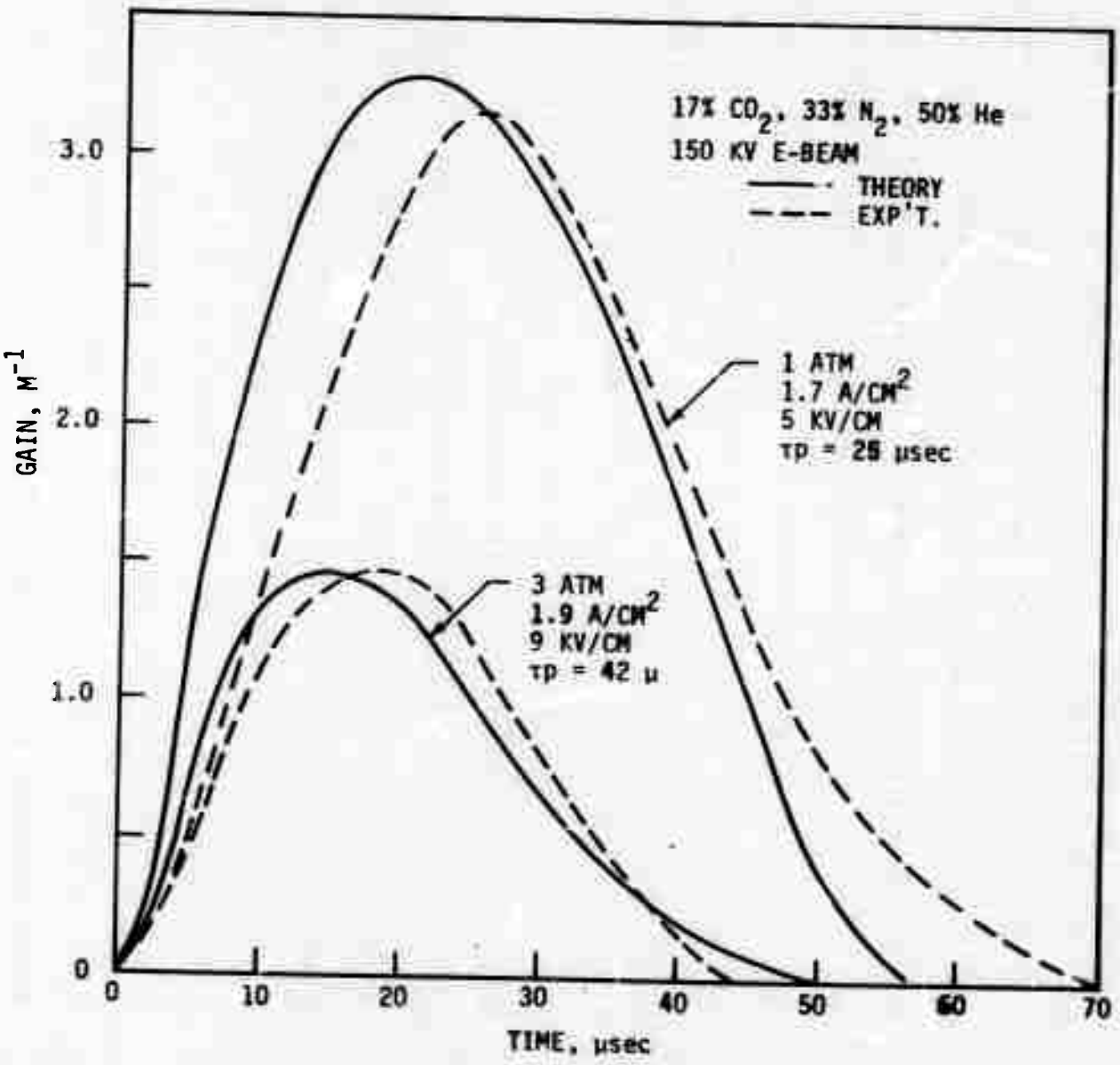

FIGURE 14. Low Signal Optical Gain in Electron Beam Stabilized Electric Discharge Laser

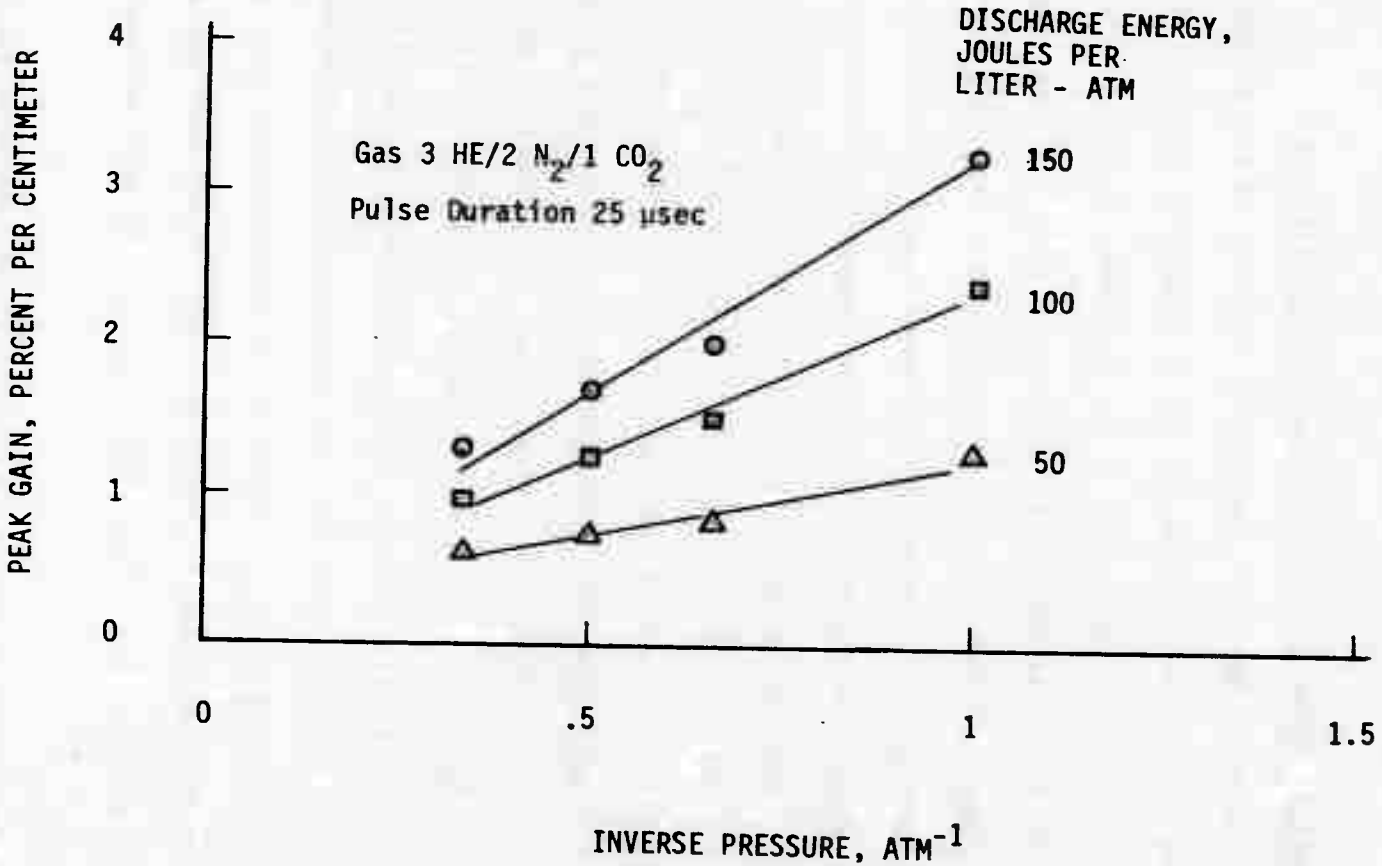

FIGURE 15. Effect of Pressure on Gain

theoretical models. At higher pressures, rotational line overlap is expected to occur which will increase the optical gain somewhat.

3.4. Optical Characteristics of Long Duration Pulses

In order to maintain good optical quality of the medium for pulse durations longer than 20 μsec, it is necessary to prevent acoustic wave motion. This requires the use of a completely confining chamber for the electrical discharge except, possibly, at the ends through which the optical beam passes. The confining chamber permits uniform gas pressure rise without wave motion. Optical disturbances then result from non-uniform heating within the volume. This occurs primarily by 3 effects:

1. The cathode fall region is heated more than other regions.
2. The cathode to foil space is not heated.
3. The regions of high electron beam current density are heated more than other regions. This is accentuated along the side walls which remove high energy electrons from the electron beam and lead to less heating adjacent to the walls.

These 3 effects have been studied experimentally and are discussed below.

The confining side walls may introduce a discharge breakdown path. However, at 1 atm pressure, it is found experimentally that a lucite wall can be introduced directly in the discharge region with no increase in the tendency to form arcs. This effect has not yet been evaluated at higher pressure.

The effect of the cathode fall on wave motion in the discharge chamber is not well documented. The effect probably depends significantly on the cathode geometry that is used. A 72 mesh per inch screen with 60 percent

porosity was used as a cathode in the present experiments. The cathode was placed at the center of the discharge chamber in full view through the optical windows. Holographic interferograms were taken of the density disturbances at various intervals during a 55 μsec pulsed discharge. The electric discharge power input was sufficient to double the total internal energy of the gas during this time. A 3 He/2 N_2/1 CO_2 gas was used at 1 atm pressure; thus a large fraction of the discharge energy was converted to heat by VT relaxation.

Two oscillograms are shown in Figure 16. Here the heated region is the larger of the 2 regions shown, and the screen is held adjacent to the heated region on a frame which blocks the optical path. No disturbance can be seen at 10 μsec, indicating that there is no appreciable pressure wave originating from the cathode fall region. This is not surprising since the cathode fall thickness is less than 10^{-3} cm at these conditions. At 55 μsec the density disturbances have propagated 2 cm in each direction and lead to a fringe shift of several CO_2 fringes per meter of path length. However the disturbances are due to isentropic waves, an expansion fan moving into the higher pressure, heated gas, and a compression wave moving into the lower pressure, unheated gas. There is no sign of a cathode shock.

A characteristics analysis of the wave motion was carried out using the CO_2 kinetics program to determine the gas temperature rise. This is compared with the experimentally measured density changes in Figure 17. The agreement between the two is within the accuracy of the measurement of the electrical power input rate per unit volume.

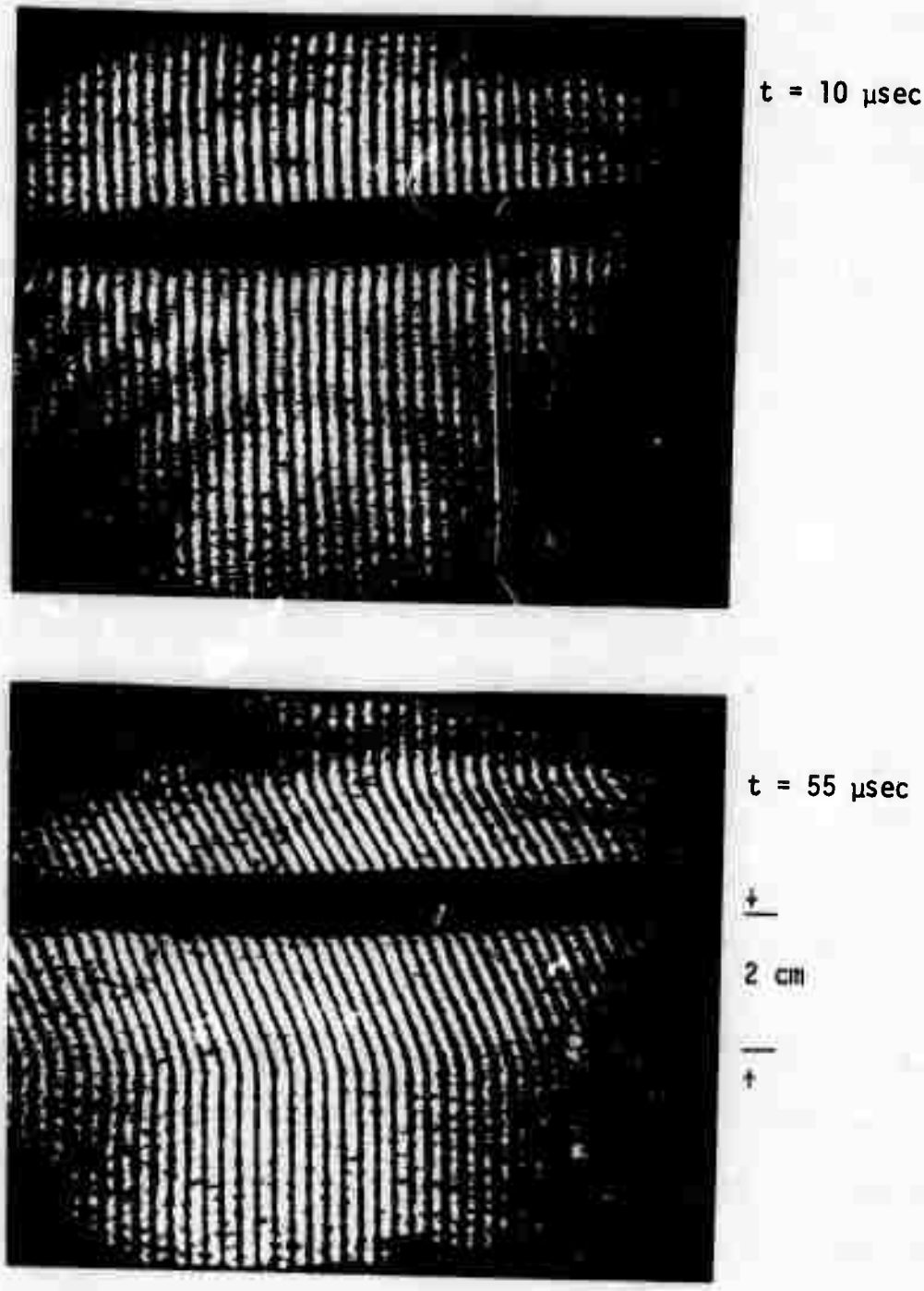

Figure 16. Ruby Holographic Interferograms of Cathode Wave Pattern
P = 1 atm 3/2/1 Mixture of $He/N_2/CO_2$
$E/P \simeq 4$ kv/cm - atm $J \simeq 1.3$ amps/cm^2

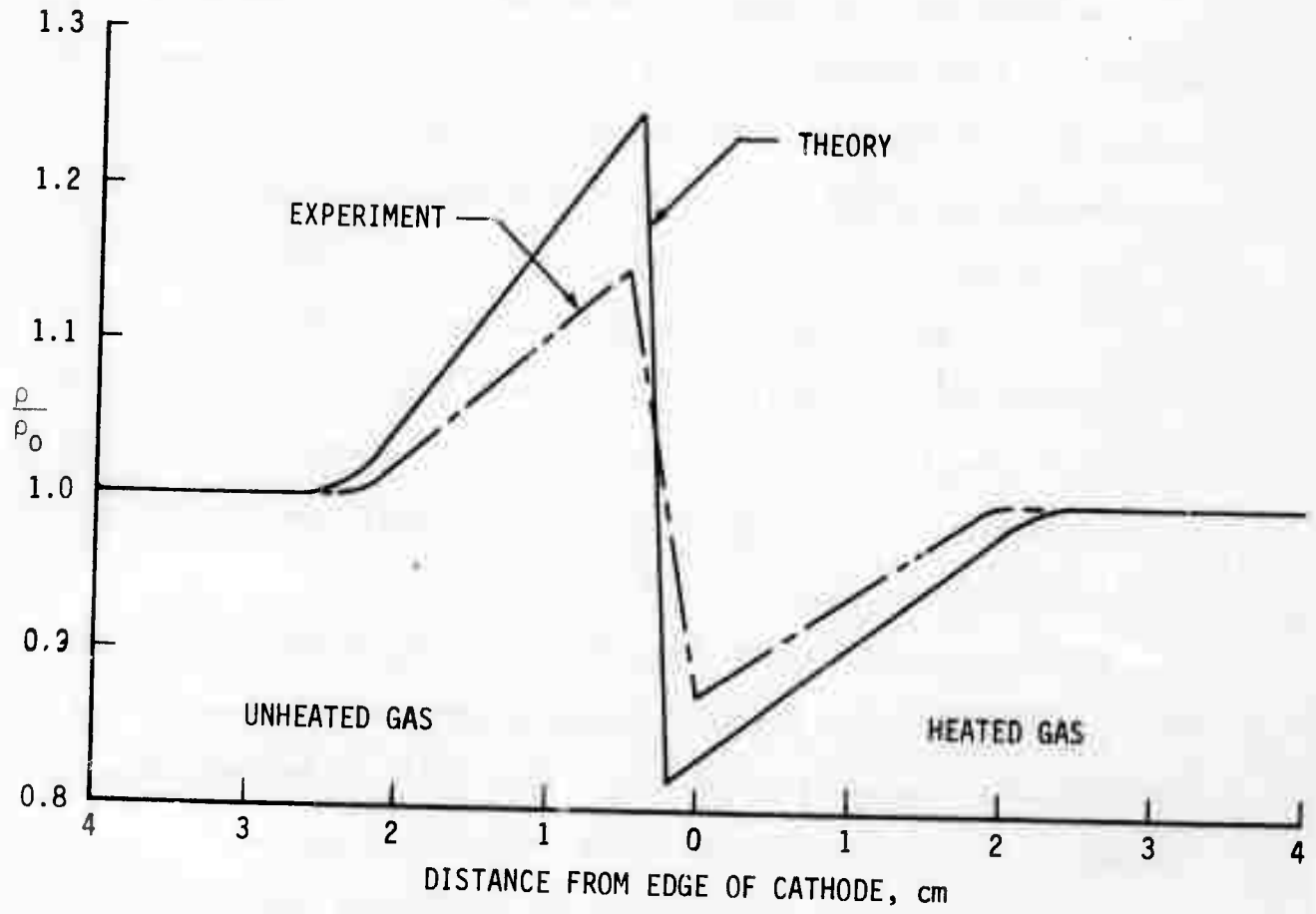

FIGURE 17. Density Profile at 55 μsec

It is concluded from this measurement that the cathode shock can be avoided by using a fine mesh screen rather than rods for the cathode. It is also clear that the void between the discharge cathode screen and the electron beam foil must be kept to a minimum or eliminated completely.

A lucite wall was placed in the heated region to study the effect of low electron beam current density near a wall. A typical experimental result is shown in Figure 18. No reference fringes were used in order to accentuate the wall effect. It is seen that the fringes are horizontal far from the wall, but curve and are vertical near the wall. Thus the region near the wall is heated less than the main discharge volume. To overcome this effect a wall material is needed that is highly reflecting rather than absorbing for high energy electrons. It will also be helpful to use high electron beam voltage and a thin electron beam foil to minimize electron beam scattering.

The effects of electron beam current density non-uniformities due to the finite tolerances required in manufacturing the electron beam equipment were also studied experimentally. This was to be done by partially blocking a portion of the electron beam using a thin foil and recording the subsequent wave pattern. Experiments were carried out with complete blocking of a portion of the electron beam. The resulting wave pattern was complex, 2 dimensional, and time dependent and could not readily be interpreted. For this reason no further effort was applied to the study of this problem.

Figure 18. Ruby Holographic Interferograms of Sidewall Wave Pattern
P = 1 atm 3/2/1 Mixture of $He/N_2/CO_2$
$E/P \simeq 4$ kv/cm - atm $J \simeq 1$ amp/cm^2

3.5. Summary of Results

It is concluded from the results of the small scale tests described here that a high pressure, long duration pulsed CO_2 laser device could be designed with confidence up to 3 atm pressure and 50 μsec pulse duration. A number of development problems require solution in connection with good optical quality for the long pulse duration; this will require experimental study of the full scale device and subsequent modification. Further research investigations are needed to develop the technology for either higher pressure or longer pulse duration operation.

SECTION IV

MULTIPLE PULSE EMISSION FROM H_2 AND N_2 ELECTRONIC STATES

As noted in Section II, a series of spikes was observed unexpectedly in the 1 to 2 micron region during the HF fluorescence observations on HF-H_2-Ar mixtures excited by electric discharges. Furthermore, when the gas mixture was changed to HF-N_2-Ar, emission spikes were also seen, but the specific wavelengths were quite different and extended from 1.5 microns to 3371 Å. Subsequent spectroscopic studies showed that the emission in HF-N_2-Ar mixtures was from N_2 electronically excited states. It is believed that the emission from HF-H_2-Ar mixtures is from H_2 electronic states although definite identification has not yet been made. In both gas mixtures it was established that HF was required in small concentration in order to obtain these emission pulses.

A manuscript describing these experimental observations has been prepared and will appear in the January 15, 1973, issue of Applied Physics Letters. This is reproduced here in Section 4.1, followed by additional experimental information. In Section 4.2 the mechanisms that may be responsible for this effect are discussed.

4.1. Experimental Observations

Laser emission has been observed previously in the IR and UV regions of the spectrum in both N_2 and H_2 by the use of either pulsed high-current high-voltage discharges (Refs. 25, 26, 27) or direct high-energy electron

beam excitation (Ref. 28, 29). Laser pulse durations observed in these experiments range from 10^{-9} sec for VUV emission to 10^{-7} sec for IR emission. The pulses generally are terminated because the lower energy levels of the laser transitions become filled (Ref. 30).

Using an electron-beam-stabilized discharge, we have observed repetitive superfluorescent pulses in mixtures of argon (89%), nitrogen or hydrogen (10%), and HF (1%). With the use of N_2, simultaneous emission pulses were seen in the IR and the UV and have been unambiguously identified as the first and second-positive bands of N_2. With the use of H_2, somewhat weaker pulses were seen in the IR and have been tentatively identified as the E, $F^1\Sigma_g^+$ (or $C^1\Pi_u$) $\rightarrow$ $B^1\Sigma_u^+$ transition of H_2. The most significant feature of the observed emission is that the pulse duration ranges from 5 to 20 μsec. This is two to three orders of magnitude longer than previously observed values and one to three orders of magnitude longer than the radiative lifetimes of the states involved. These long-duration pulses were not observed when HF was removed from the gas mixture and were not readily obtained when Ar was removed.

A large-area thermionic cathode electron beam (Ref. 31), operated at 125 kV, was used in these experiments to provide a stable high-pressure electric discharge for a time of 20 - 40 μsec. The electron beam provided a current density of up to 4 mA/cm^2 through a 0.04-mm-thick high-strength aluminum foil. A cylindrical Teflon discharge chamber was used with calcium fluoride windows mounted opposite each other, 21 cm apart. A 4 x 15-cm aluminum screen was used as the discharge cathode. A 50-Ω copper sulfate resistor was used in series with a spark-gap triggered capacitor (0.4 μF)

to supply current at 5 - 10 kV across a 7-cm gap in the chamber. An operating pressure of 200 Torr was generally used. A Jarrell-Ash 0.25-m Ebert spectrometer, equipped with both 6000-Å and 2.1-μ blazed gratings, was used for spectral measurements, together with a liquid-nitrogen-cooled Ge:Au detector for the near IR and a 1P28 photomultiplier for the UV-visible portion of the spectrum. The rise time of each detector was less than 1 μsec.

Argon (Airco, 99.995%), hydrogen (Airco, 99.999%), and nitrogen (Airco, 99.99%) gases were used without further purification. HF supplied by Matheson was purified by distillation at liquid-nitrogen and chloroform slush temperatures and held in a monel cylinder. Vacuum lines were constructed of monel and passivated at 1 atm of chlorine trifluoride. A short length of polyethylene tubing connected the monel vacuum system to the Teflon test section. The HF was used from the monel storage vessel at an HF pressure of 500 Torr and mixed with the Ar/N_2 or Ar/H_2 gas in a flowing system. The test-cell filling rate was approximately 350 Torr/min. Exit gases were passed through a liquid-nitrogen-cooled trap. The gas temperature and pressure in the test section were maintained at 20° C and 200 Torr, respectively.

Figure 19 illustrates the repetitive superfluorescent pulses observed at 3370 Å in N_2. The behavior is very similar to that seen for H_2 and N_2 in the near IR. By scanning 30 Å to either side of the 3370-Å emission, no pulsed output was observed. Table IV-1 lists the other wavelengths at which maximum superfluorescent emission was observed. The emission is characterized by a sharp initial pulse at the onset of the electrical

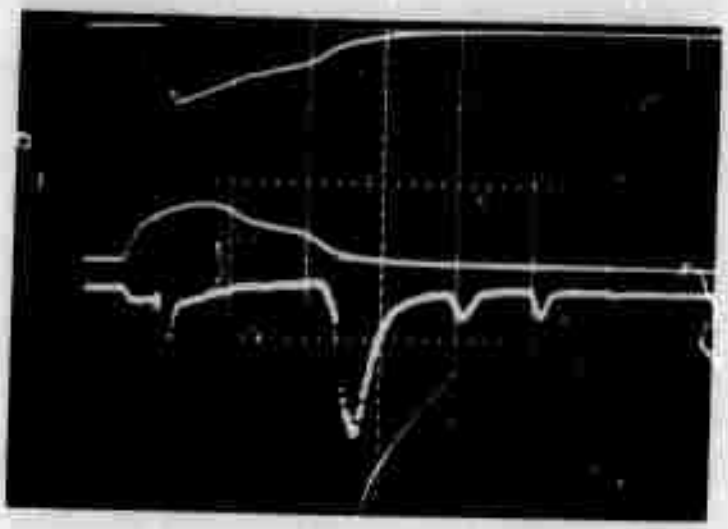

Figure 19. Superfluorescent pulses at 3370 Å in a mixture of 10% N_2, 89% ar, and 1% HF at 200 Torr pressure. The sweep speed is 20 μsec/div. The initial capacitor voltage is 11 kV. The upper trace is the total discharge current through a 57.5-cm^2 area (100 A/div), the middle trace monitors the relative electron-beam current, and the lower trace (signal increasing downward) is the relative fluorescent emission at 3370 Å with a 5-Å spectral slit width.

Table IV-1

Locations of Peak Superfluorescence in N_2 and H_2

$N_2(B^3\pi_g \rightarrow A^3\Sigma_u^+)$ First-Positive System		$N_2(C^3\pi_u \rightarrow B^3\pi_g)$ Second-Positive System		$H_2(E,F^1\Sigma_g^+$ or $C^1\pi_u \rightarrow B^1\Sigma_u^+)$	
Wavelength[a]	Assignment (v', v")	Wavelength[b]	Assignment (v',v")	Wavelength[a]	Assignment (v',v")
1.04 μ	0,0	3370 Å	0,0	1.50 μ	0,2 P(4)[c]
1.23 μ	0,1	3576 Å	0,1	1.63 μ	0,3 P(6)[c]
1.48 μ	0,2	3804 Å	0,2		
		4058 Å	0,3		

[a] 0.02 μ spectral slit width.

[b] 5 Å spectral slit width.

[c] Tentative assignment.

discharge, during a period of high E/p and low current, followed by a series of long-duration pulses during the decay of the discharge when the electron-beam current is terminated. The intensity and frequency of the long-duration pulses increase (roughly linearly) as the HF concentration is increased from 0.75 to 3%.

In Figure 20 the near-IR emission from the nitrogen first-positive system is shown with the use of a semiconfocal resonator with internal gold-coated mirrors and a 1-mm-diameter output coupling hole. An active discharge length of 15 cm was used between the mirrors. It was found that the mirrors enhanced the intensity of the long-duration pulses by an order of magnitude over the background radiation, which confirmed the presence of optical gain at this wavelength.

The electron beam alone did not produce any detectable superfluorescent pulses. A threshold value of E/p was observed both for the initial pulse and the long-duration pulses. The superfluorescent pulse intensity increased with increasing E/p until arc formation prematurely terminated the electrical discharge. The arc formation occurred earlier as the HF concentration was increased. The discharge current during the superfluorescent pulse output ranged from 0.2 to 1.0 A/cm^2, and the values of E/p ranged from 3 to 5 kV/cm atm.

The spectroscopic data in the 1 to 2 micron region obtained in HF-N_2-Ar and HF-H_2-Ar mixtures are shown in Figures 21 and 22. For N_2 the identification with the first positive band is quite clear. For H_2 the spectrum is more diffuse, probably because of the large rotational constant of H_2, and the identification is less certain.

Figure 20. Optical-cavity emission in the ir from a 10% N_2, 89% Ar, 1% HF mixture at 200 Torr pressure. The sweep speed is 20 μsec/div. The initial capacitor voltage is 12 kV. The upper trace is the total discharge current through a 57.5-cm^2 area (100 A/div), the middle trace monitors the relative electron-beam current, and the lower trace is the total ir emission observed through a 1-mm output coupling hole using a Ge:Au detector. A small initial-emission spike is seen at the onset of the discharge current. A 10-μsec duration emission pulse is seen as the discharge current decays following termination of the electron-beam current. This is followed by an arc in the discharge region. Both emission pulses were identified as belonging to the first-positive band of N_2.

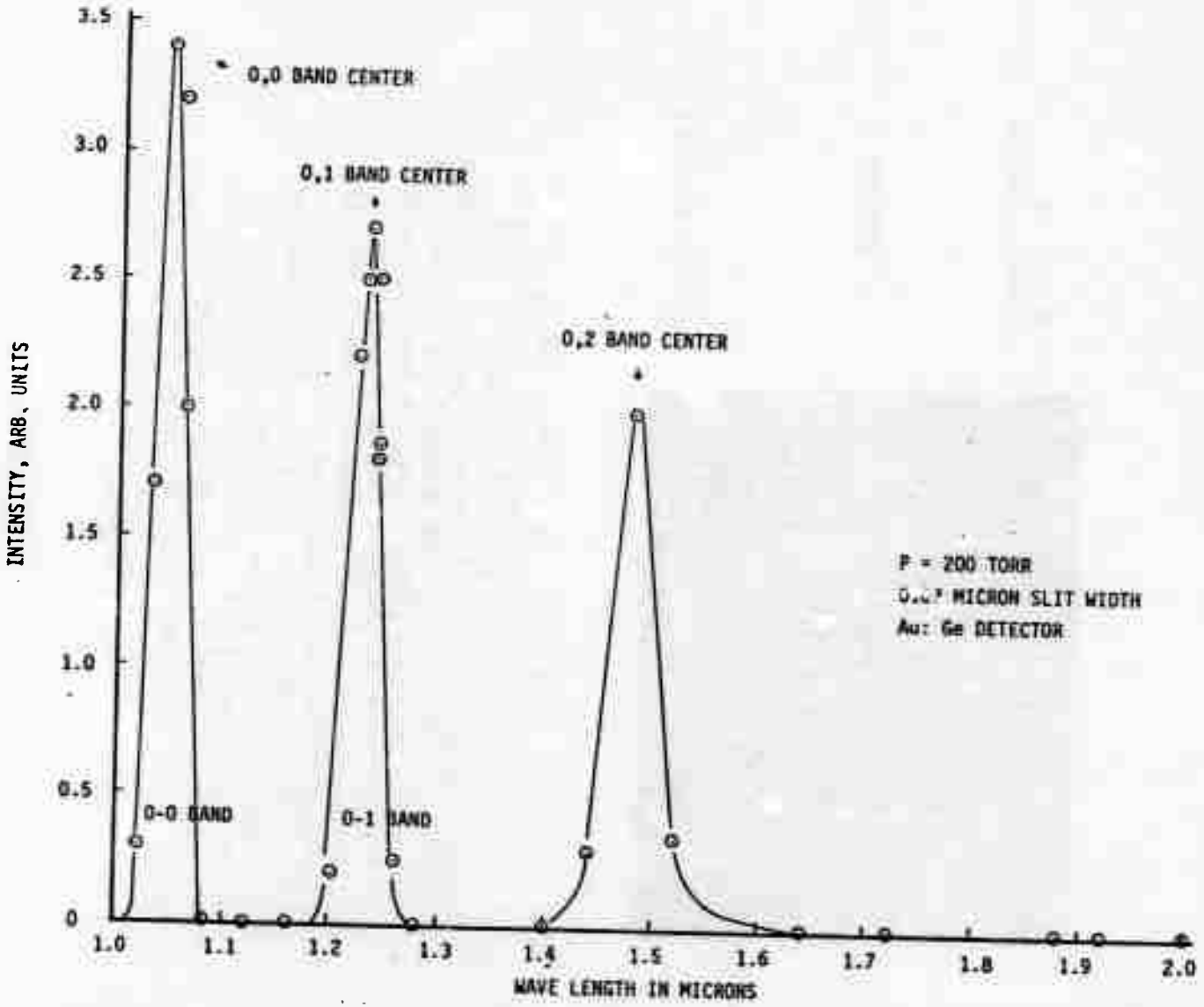

FIGURE 21. Spectral Distribution of Nitrogen First Positive Superradiance in 1.5% HF, 10% N_2, 88.5% Ar

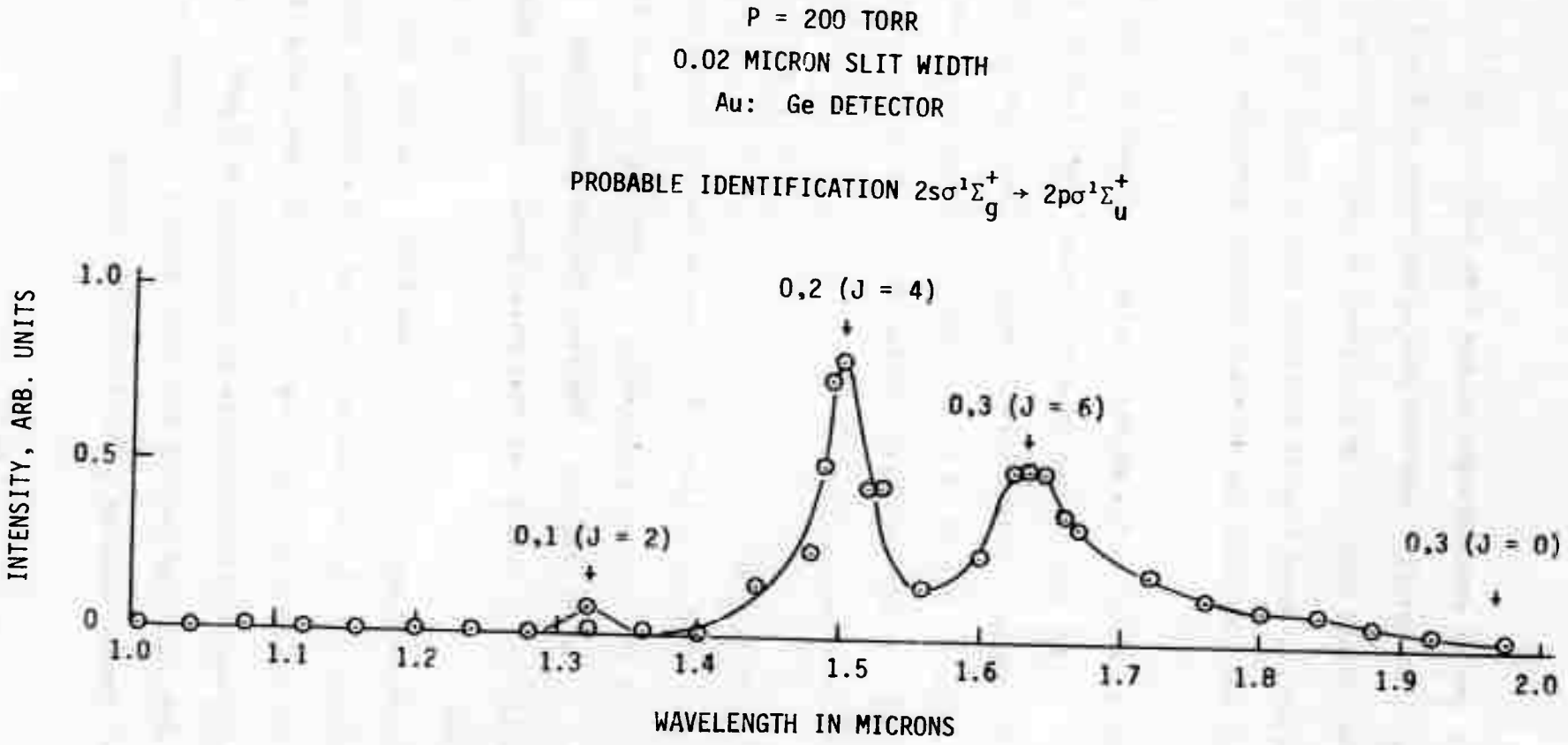

FIGURE 22. Spectral Distribution of Hydrogen Superradiance in 1.5% HF, 10% H_2, 88.5% Ar

The effect of the HF concentration on the time interval and the amplitude of the N_2 first positive emission pulses are shown in Figure 23. The interval is roughly inversely proportional to the HF concentration and the amplitude increases roughly in proportion to the HF concentration. At the highest amplitude the detector circuit approaches saturation.

In an attempt to suppress the emission spikes, the internal reflectivity of the test cell was reduced by using Nextel flat black paint. It was found that the emission spikes were increased rather than suppressed and that they appeared with no HF in the flow. This indicates that volatile hydrocarbons may have an effect similar to that of HF in causing these repetitive emission pulses.

4.2. Interpretation of Results

The effects described in Section 4.1 are quite new and unexpected. At present there is no theoretical explanation or quantitative model with which these results could be compared. The data indicate that electron impact excitation is very important and that collisional processes involving HF are important.

The N_2 fluorescence spikes occur on transitions which are well known to produce laser oscillation, but at considerably different conditions and for a very short time (less than 1 μsec). The short pulse N_2 laser is produced by an electric discharge at considerably higher voltage than used here. The discharge excites the upper electronic states of N_2 by electron impact faster than the lower electronic states.

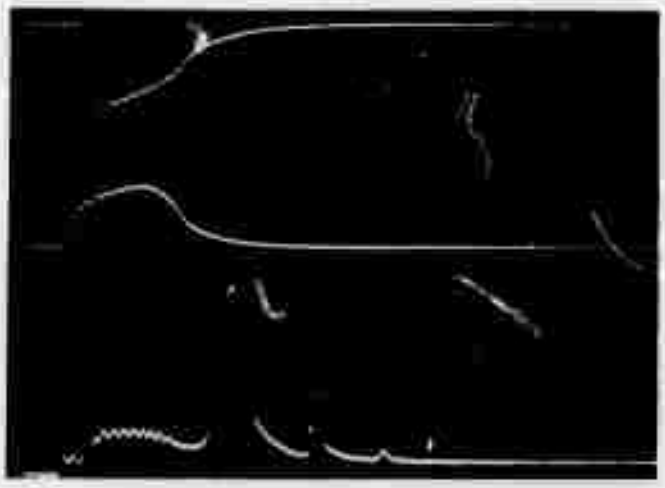

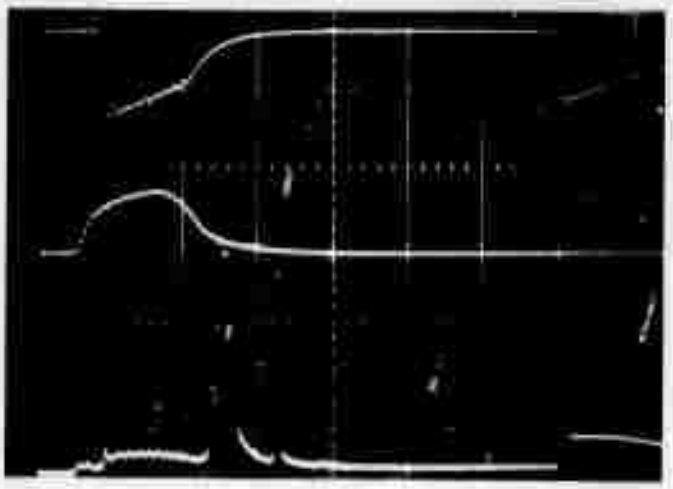

Figure 23. Fluorescence in 10% N_2, 90% Argon with Trace HF
P = 200 Torr E/P = 3 kv/cm - atm 20 μsec/cm
1 to 11 Microns 57.5 cm^2 Cathode Area

As stimulated emission rises, the rate of populating the lower states rises until the inversion is finally lost by the filling of the lower electronic states.

This process could be stretched in time if the HF molecule were significant in removing the lower electronic states. In the case of the N_2 first positive band the lower laser level is the lowest metastable state, $A^3\Sigma_u^+$. One possibility is the electronic transfer from $N_2(A^3\Sigma_u^+)$ to a repulsive electronic state of HF which leads to dissociation. However the $N_2(A^3\Sigma_u^+)$ electronic energy is only slightly greater than the dissociation energy of HF, whereas the only known vacuum uv absorption continuum of HF is at 1400 Å.

A second possibility is the efficient vibrational quenching property of HF. A mechanism may be found which involves two temperatures, a high electron temperature that is maintained by the electric field, and a low vibrational temperature that is maintained close to the translational temperature by VT relaxation in collisions with HF or another molecule that serves as a vibrational decay catalyst. This may occur on the second positive band system by the two steps

electronic transfer: $N_2(B^3\pi_g) + N_2 \rightarrow N_2(A^3\Sigma_u^+)^{VIB} + N_2$

vibrational quenching: $N_2(A^3\Sigma_u^+)^{VIB} + HF \rightarrow N_2(A^3\Sigma_u^+) + HF$

However, in order to compete with the $N_2(C^3\pi_u)$ spontaneous decay lifetime under the experimental conditions used here, the HF vibrational quenching probability must be close to 1.

It is clear from the foregoing discussion that the mechanism responsible for the observed fluorescent pulses is not yet understood. However, the potential of the possibilities discussed here warrants further investigation.

REFERENCES

1. C. A. Fenstermacher, M. Nutter, W. Leland, and K. Boyer, Appl. Phys. Lett. 20, 56(1972).

2. J. D. Daugherty, E. R. Pugh, and D. H. Douglas-Hamilton, "A Stable Scalable, High Pressure Gas Discharge as Applied to the CO_2 Laser," presented at the 24th Annual Gaseous Electronics Conference, Gainsville, Florida, October 1961.

3. K. L. Kompa, J. H. Parker, and G. C. Pimentel, J. Chem. Phys. 49, 4257 (1968).

4. J. H. Parker and G. C. Pimentel, J. Chem. Phys. 51, 91 (1969).

5. M. L. Bhaumik, W. B. Lacina, and M. Mann, IEEE J. Quant. Electron, QE-6, 576 (1970); R. E. Center and G. E. Caledonia, Appl. Phys. Letters 19, 211 (1971).

6. R. C. Millikan and D. R. White, J. Chem. Phys. 39, 3209 (1963).

7. J. Bott, J. Chem. Phys. 57, 96 (1972).

8. J. J. Hinchen, United Aircraft Report UAR-L127, July 1972.

9. H. L. Chen and C. B. Moore, J. Chem. Phys. 54, 4072 (1971).

10. P. F. Zittel and C. B. Moore, "V→T,R and V-V Relaxation in DCl Systems," to be published in J. Chem. Phys.

11. E. Linder and H. Schmidt, Zeitschrift fur Naturforschung, Band 26a, Heft 10, 1064 (1971).

12. G. J. Schulz, Phys. Rev. A135, 988 (1964).

13. H. S. W. Massey, Electronic and Ionic Impact Phenomena, Vol. II (Oxford University Press, Clarendon, 1969), p. 888.

14. H. S. W. Massey, loc. cit., p. 1063.

15. G. E. Caldeonia and R. E. Center, J. Chem. Phys. 55, 552 (1971).

16. R. J. Lovell and W. F. Herget, J. Opt. Soc. Am. 52, 1374 (1962).

17. D. F. Smith, Molecular Properties of Hydrogen Fluoride, 2nd UN Geneva Conference, Pergammon Press, London

18. B. Oksengorn, Spectrochimica Acta, Vol. 19, 541 (1963).

19. C. J. Ultee, Rev. Sci. Inst. 42, 1174 (1971).

20. W. H. Green and M. C. Lin, I.E.E.E. J. Quant. Elect., QE-7, 98 (1971).

21. A. G. Englehardt and A. V. Phelps, Phys. Rev. A133, 375 (1964).

22. Byron, S., et al., High-Energy Pulse Generation, Final Report AFWL-TR-70-151, Air Force Weapons Laboratory, Kirtland AFB, New Mexico, July 1971.

23. A. L. Hoffman and G. C. Vlases, IEEE J. Quant. Elect., QE-8, 46 (1972).

24. W. H. Christiansen, "Pulsed Gasdynamic Lasers," AIAA 4th Fluid and Plasma Dynamics Conference, Palo Alto, California, June 21-23, 1971.